Shock-wave viscosity measurement

Gregory H. Miller* and Thomas J. Ahrens

Helen E. Lindhurst Laboratory of Experimental Geophysics, Division of Geological and Planetary Sciences, California Institute of Technology, Pasadena, California 91125

The problem of measuring the viscosity of fluids under shock-loading conditions is discussed. The authors examine in detail the method of Sakharov *et al.* (1965) and Zaidel' (1967) for measuring shear viscosity from the decay of perturbations on a corrugated shock front. The relevance of initial conditions, finite shock amplitude, bulk viscosity, and the sensitivity of the measurements to the shock boundary conditions are discussed. The validity of the viscous perturbation approach is examined by numerically solving the second-order Navier-Stokes equations. These numerical experiments indicate that shock instabilities may occur even when the Kontorovich-D'yakov stability criteria are satsified. The corrugated shock front induces mixing of the shocked sample. This mixing is particularly vigorous in viscous materials and may be responsible for the rapid rate of some shock-induced chemical reactions. The experimental results for water at 15 GPa are discussed, and several possibilities are considered to explain why the viscosity obtained by these experiments is so different from those obtained by other methods. Two possible reasons are favored: (1) the analytic method may be inappropriate because it ignores possible complications at the onset of the shock perturbations, and (2) the large effective viscosity determined by this method may reflect the existence of ice VII on the Rayleigh path of the Hugoniot. The latter interpretation reconciles the experimental results with estimates and measurements obtained by other means and is consistent with pressure-volume-temperature Hugoniot data and the phase diagram of H_2O.

CONTENTS

I. INTRODUCTION

The viscosity of the Earth's metallic liquid outer core has been called one of the most important, and least well determined, of all geophysical parameters (Merrill and McElhinny, 1983; Jacobs, 1987). Estimates of its viscosity span some 13 orders of magnitude (Rochester, 1970). These estimates have been made on the basis of scaling theories (e.g., 3.7×10^{-2}–18.5×10^{-2} poise; Gans, 1972), extrapolation of low-pressure experimental values for liquid mercury (e.g., 500 poise; Backus, 1968), and the attenuation of seismic waves (e.g., 3×10^{7}–7×10^{7} poise; Suzuki and Sato, 1970). At present, the direct experimental measurement of the viscosity of liquid metals at outer core pressures ($\approx$136–329 GPa) and temperatures ($>$4000 K) exceeds the capabilities of modern laboratory techniques. Shock-wave methods have been devised, however, that may potentially address this problem.

The viscosity of high-pressure silicate liquids is one of the fundamental parameters that controls rates of chemical fractionation and heat transport in the Earth. Most magmatic activity is thought to occur in the shallow upper mantle and crust of the Earth, in a pressure regime ($<$3 GPa) that is experimentally accessible by conventional piston-cylinder techniques. However, several theories for the origin and early evolution of the Earth postulate that magmatic activity may have extended to the core (e.g., Melosh, 1990). Some refractory volcanic rocks (komatiites) are also postulated to have originated at great depths within the mantle (Miller *et al.*, 1991). Detailed evaluation of these hypotheses is reliant on a knowledge of the viscosities of silicate liquids at pressures that are currently inaccessible to piston-cylinder techniques. Again, shock-wave methods may provide the solution.

The foremost theoretical model for the viscosity of liquids is the Enskog model (Hansen and McDonald, 1986), which is based on the properties of a hypothetical hard-sphere fluid. Such a fluid would be composed of rigid, spherical particles like those Democritus postulated in the third century B.C., rather than the structured atoms with which we are familiar. The Enskog model predicts a systematic increase in both shear and bulk viscosity with increasing compression. Molecular dynamic simulations of hard-sphere fluids (Alder *et al.*, 1970) generally support the Enskog theory, particularly for the bulk viscosity, but predict significant deviations for the shear viscosity as the density of the liquid approaches that of a close-packed solid. This deviation is

*Now at Department of Geology and Geophysics, University of California, Berkeley, CA 94720.

attributed to the molecular chaos treatment of many-body correlations in the Enskog theory. The molecular chaos approximation supposes that the autocorrelation function decays exponentially with time. The molecular dynamic simulations indicate a more gradual decay in the autocorrelation function, like $t^{-3/2}$, showing the existence of slowly decaying collective motions in the hard-sphere liquid. The bulk viscosities calculated for hypothetical liquids described by the softer Lennard-Jones potential also deviate from the Enskog theory (Hoover, Evans, *et al.*, 1980; Hoover, Ladd, *et al.*, 1980). Still greater deviations are predicted by simulations of multicomponent liquids with more realistic potential interactions.

The systematics of liquid silicate viscosity with pressure are believed to be complex. Molecular dynamics studies on liquid silicates (Woodcock *et al.*, 1976; Angell *et al.*, 1982) predict that viscosity will diminish with increasing pressure to a minimum value in the neighborhood of 25 GPa and increase thereafter. This anomalous behavior is attributed to the idea that liquid silicates undergo an increase in mean coordination number with increasing pressure, which increases interatomic distances and thereby reduces the viscosity. Once the coordination changes are complete (near 25 GPa), additional increases in pressure will reduce interatomic distances, causing viscosity to increase. Static-pressure viscosity measurements to 3 GPa (e.g., Kushiro, 1980) confirm this trend, although the predicted minimum remains experimentally inaccessible by this method. Order-of-magnitude viscosity changes with temperature (Bottinga and Weill, 1972) and pressure (e.g., Kushiro, 1986) have been detected in silicate liquids (see also the comprehensive review of Ryan and Blevins, 1987). This sensitivity of viscosity to both pressure and temperature demonstrates that extrapolation of low-pressure and/or low-temperature measurements to high-pressure high-temperature conditions of geophysical interest is subject to very large uncertainties. This is particularly true in silicate systems where liquid-state structural changes have been inferred (e.g., Rigden *et al.*, 1988; Knittle and Jeanloz, 1989).

A variety of experimental methods have been employed to determine the viscosity of liquids at high pressure. Under static high-pressure conditions, the Stokes drag on falling spheres (Kushiro, 1976, 1977, 1978a, 1978b, 1978c, 1980, 1986; Kushiro *et al.*, 1976; Fujii and Kushiro, 1977a, 1977b; Scarfe *et al.*, 1979; Kanzaki *et al.*, 1987) has been measured to simultaneously determine the density and shear viscosity of liquids to pressures of 3 GPa. Dynamic high-pressure (shock-wave) experiments can be used to access a greater range of pressures and temperatures. These shock-wave methods fall into three general categories.

First, the rise time or width of the shock front can be related to some effective viscosity averaged over the range of pressures, temperatures, and compression experienced by the sample in this shock-front region (e.g., Landau and Lifshitz, 1959, pp. 337–341; Bland, 1965; Zel'dovich and Raizer, 1967, pp. 468–482). The basic idea here is that the shock-front thickness (for strong shocks) is on the order of a few mean free paths of the thermal motion of the shocked material. Viscosity, which is also proportional to the mean free path, is therefore proportional to the shock-front thickness. The rise of the shock front can be experimentally determined with high precision using velocity interferometry techniques (see, for example, Barker, 1968) or capacitive rate gauges (e.g., Razorenov *et al.*, 1987; other methods are described in Grady, 1977) and can be related to viscosity (e.g., Swegle and Grady, 1985). Because this method determines the viscosity over the very broad range of conditions experienced in the shock front, and because the strain rates in this region are exceedingly large, this method may be inappropriate for determining the low-frequency, i.e., relaxed, viscosity of the high-pressure state.

Second, indirect indicators of viscosity have been used to estimate the viscosity of materials at high pressure. These indirect indicators include fluorescence lifetimes in glycerine (Huston *et al.*, 1985), electrical conductivity measurements of weak electrolyte solutions (Hamann and Linton, 1969), and the diffusion-controlled precipitation of sulfur in thiosulphate solutions (Yakusheva *et al.*, 1972). The fluorescence method is based on the observation that the fluorescence lifetime of the crystal-violet (CV) dye molecule is correlated to the $\frac{2}{3}$ power of the viscosity of the glycerine solvent (Förster and Hoffmann, 1971), both for viscosity variations achieved by changing pressure and for those achieved by changing temperature (Brey *et al.*, 1977). This special feature of the CV-glycerine system is critical to the success of this method, since pressure and temperature vary simultaneously under shock compression. The conductivity method is based on the theoretical argument, Walden's rule (Walden, 1906), that the product of ionic conductivity and viscosity is a constant for a given system. These methods can, in principle, sample the low-frequency viscosity, but they rely critically on the validity of the calibrations that link the measured properties to viscosity. For well studied systems, where viscosity and conductivity or fluorescence kinetics have been independently measured as functions of pressure and temperature, these indirect indicators can be applied in shock-wave experiments. Such methods are inherently suspect outside the pressure/temperature range of static experiments, where the validity of the calibrations cannot be assured.

Third, direct measurements of high-pressure viscosity are possible by observing induced flows in high-pressure materials. These experiments include the measurement of the oscillatory damping of a sinusoidal shock front (Sakharov *et al.*, 1965; Mineev and Savinov, 1967, 1976; Mineev and Zaidel', 1968) and measurement of the viscous drag on an embedded cylinder (Al'tshuler *et al.*, 1977, 1986; Kim, 1984). These methods require no calibration, since they are based on directly measuring variables associated with the fluid mechanics of viscous flow.

In the viscous drag experiment, a metal cylinder is em-

bedded in a nonconductive sample, oriented parallel to the plane of the shock. When the sample is shocked, the cylinder is accelerated. The initial acceleration is complicated by shock-wave interactions, but after a short time the acceleration is controlled by the viscous drag of the sample flowing past the cylinder. The velocity of the cylinder, measured by detecting electrical current induced by the motion of the metal cylinder in a magnetic field, is recorded as a function of time. This velocity history is analyzed with a simple viscous flow model to give the sample's shear viscosity. Because velocity is detected by measuring electrical currents, this technique requires a nonconductive sample. The oscillatory damping experiment is insensitive to the conductivity of the sample and is therefore applicable to a greater variety of materials. The oscillatory damping experiment is the principal focus of this study.

The oscillatory damping experiment is elegant in its simplicity. Figure 1 illustrates the experimental apparatus of Sakharov *et al.* (1965). An explosive block is used to drive a shock into a disc of sample material in which a series of sinusoidal grooves are cut. When the shock intersects these grooves a sinusoidal perturbation is created on the shock front. This perturbed shock then propagates into a wedge of sample material. The curvature of the shock front generates velocity perturbations in the compressed sample. These velocity perturbations, modified by the sample viscosity, are coupled with the wave front. The shock-front fluctuations are therefore direct indicators of the shocked-fluid viscosity. The wedge shape of the sample allows the amplitude of the shock-front perturbations to be examined as a function of time. The shock profile is detected by using a streak camera to record light flashes induced by the shock's arrival between the top surface of the wedge and the overlying plastic buffer (Fig. 2).

In contrast to the simplicity of this experimental design, the analysis of these experiments is very complex, as is evident in the work of Zaidel' (1967). In the particular case of shocked water, this method gives consistently high values of viscosity relative to other methods (Fig. 3): by a factor of 10^6 relative to the conductivity method, and by a factor of 10^3 relative to the viscous drag method (Al'tshuler *et al.*, 1986). The disagreement with the viscous drag experiments is not easily explained, but the former discrepancy has been attributed to the failure of Walden's rule at high pressure (Al'tshuler *et al.*, 1986). However, these conductivity results are broadly compatible with extrapolation of static-pressure falling sphere measurements to 10 kbar (Bett and Cappi, 1965). These static-pressure experiments indicate that water has a temperature-dependent minimum viscosity in the neighborhood of 0–2 kbar. At 20 °C, the viscosity at 10 kbar is only twice its 1 bar value of 1.0×10^{-2} poise.

It is possible that the analytic method of Zaidel' (1967) is correct and that water does exhibit a near-solid rheology at high pressure. Alternatively, errors in the analytic method may have led to a misinterpretation of the experiments. It is also possible that the experiments did not

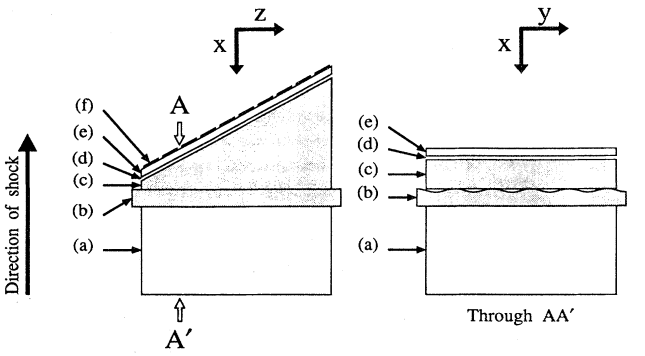

FIG. 1. Schematic of experimental design. An explosive assembly (a) generates a shock that first enters a sinusoidally grooved sample disc (b). The sinusoidal grooves generate perturbations in the shock front that then propagate into the sample wedge (c). The profile of the shock front is detected as a function of time by the light emitted upon shocking a thin gap filled with a noble gas such as argon [flash gap, (d)] by the arrival of the shock at the free surface of the wedge. The emitted light is shuttered by the shock-induced opacity of a plastic sheet (e), and a mask (f).

adequately realize the initial conditions presumed in the analysis (Godunov *et al.*, 1971). The viscosities of shocked solids determined by this method, however, are in substantially good agreement with estimates obtained through the study of the shock-welding phenomenon (Godunov *et al.*, 1971). In these shock-welding experiments, two like metal plates are welded together in an oblique impact driven by an explosive charge. Markers, inserted into the plates prior to impact, are deformed during the welding process. These markers are then examined in thin sections cut from the post-shock specimens and show the existence of approximately parabolic deformation gradients near the plane of the weld. Assuming these gradients are accurate records of the flow field of the viscous jets, and given an estimate of the contact angle and contact point velocity, these experiments can be modeled with the incompressible, viscous Stokes equation to give a shear viscosity of the jetting metals.

The melting of aluminum along the Hugoniot has also been detected by associated decreases in viscosity (Mineev and Savinov, 1967) by the Sakharov *et al.* (1965) method and is in agreement with independent theoretical determinations of the high-pressure fusion curve.

In this paper we examine the analytic method in greater detail and augment the treatment of Zaidel' (1967) by considering some alternative approximations. First the boundary conditions at the shock front are derived in Sec. II. The initial conditions are discussed briefly in Sec. III. Next, the linearized equations of motion and continuity are developed in Sec. IV. The shock perturbation development solution follows in Sec. V in the inviscid limit. A viscous perturbation follows in Sec. VI, and again in Sec. VII with the different set of boundary conditions proposed by Zaidel' (1967).

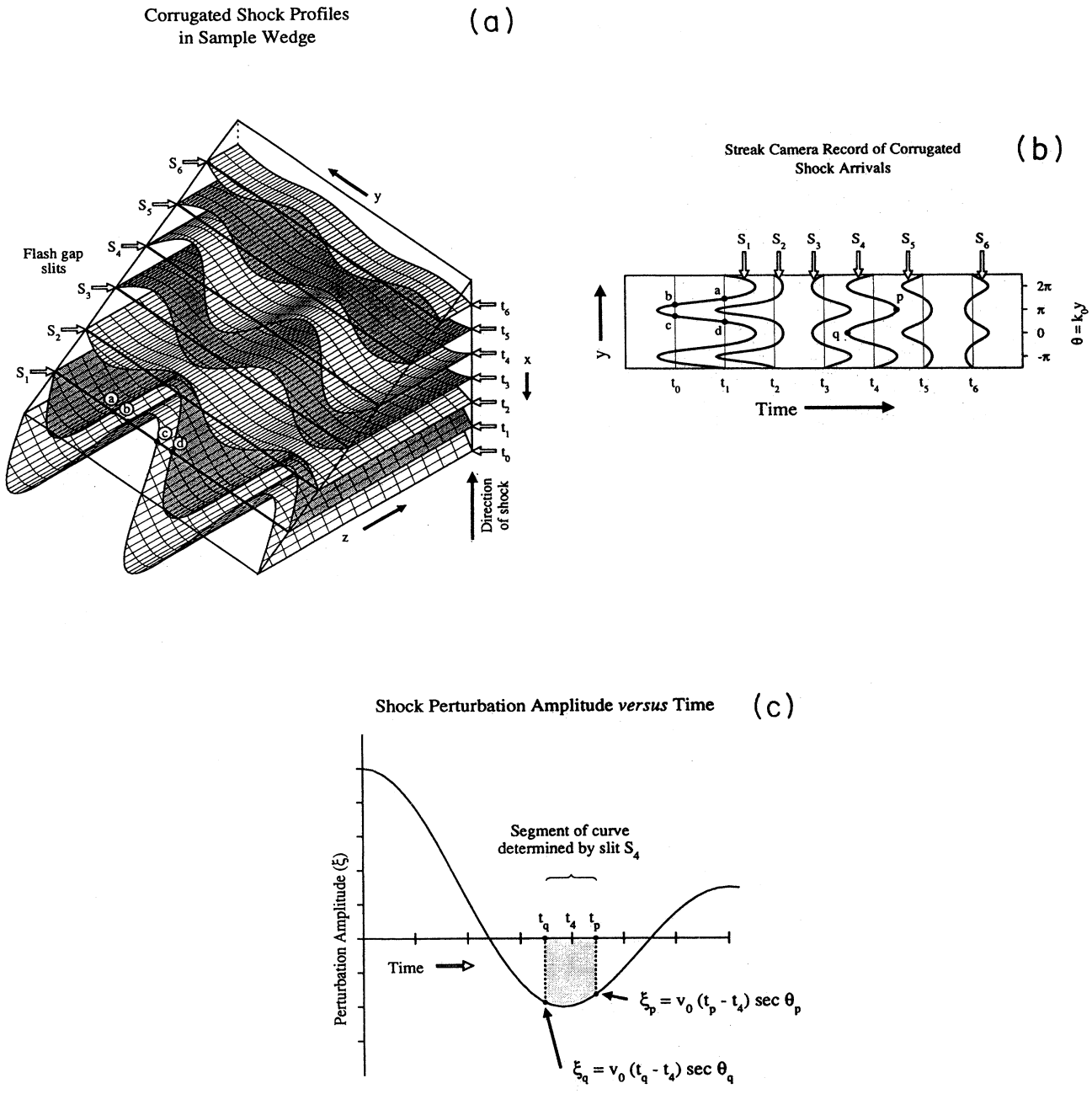

FIG. 2. (a) Diagram of corrugated shock wave at several times ($t_0 < t_1 < t_2 < t_3 < t_4 < t_5 < t_6$) as it propagates through the sample wedge (Fig. 1). Slash gap slits (S_1, S_2, S_3, S_4, S_5, and S_6) are shown across the top surface of the wedge. When the shock front intersect the slits, a brief flash of light is emitted that can be recorded on a streak camera. A streak camera image of these slits is shown in (b). Consider the slit S_1. At time t_0, the shock front intersects the slit at points "*b*" and "*c*" (and two other unlabeled points). Slit S_1 will be illuminated on the streak camera record [Fig. 2(b)] at time t_0 at these points of intersection. Similarly, the points "*a*" and "*d*" represent the intersection of the shock front at time t_1 with slit S_1. Slit S_1 is illuminated on the streak camera record at time t_1 at the points "*a*" and "*d*" [Fig. 2(b)]. The slit images on the streak camera record may additionally be geometrically offset along the time axis. (c) The streak camera record can be inverted to give the amplitude of the shock-front corrugation as a function of time. Consider the point "*p*" on the slit S_4 record. This point was generated at time t_p by a corrugated shock whose amplitude is $\xi(t_p)\cos(k_0 y)$. The distance traversed by a plane shock in the interval t_4 to t_p is $v_0(t_p - t_4)$ where v_0 is the shock-wave velocity (U_S) in the laboratory reference frame. This distance is equal to the amplitude of the perturbation $\xi(t_p)\cos(k_0 y_p)$; thus the shock amplitude at time t_p is $v_0(t_p - t_4)\sec(k_0 y_p)$. Point "q" is is similarly inverted on Fig. 2(c). The shaded region is the range of values that can be determined from points on the slit S_4 record.

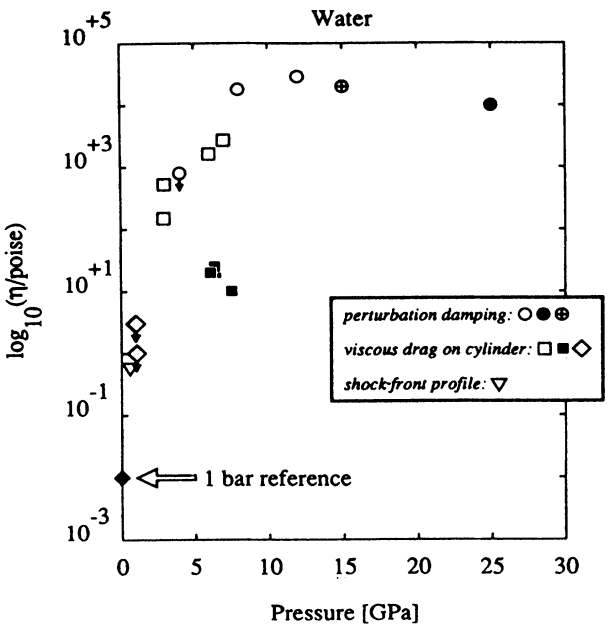

FIG. 3. Summary of shock-wave viscosity measurements on water: ○, Mineev and Zaidel' (1968); ●, Mineev and Savinov (1976); □, Al'tshuler *et al.* (1977); ■, Kim (1984); ◇, Al'tshuler *et al.* (1986); and △, shock thickness measurement of Harris and Presles (1981). The crossed circle indicates our new interpretation of the Mineev and Zaidel' (1968) 15 GPa experiment calculated with approximate initial conditions and assuming $\kappa=\eta$. The viscosity calculated by Mineev and Zaidel' lies within the crossed circle. Symbols with arrows denote upper bounds.

In Sec. VIII a summary of approximations is presented and their impact is discussed. In Secs. IX and X the initial conditions are reexamined and a semiquantitative initial-condition model is introduced. In Sec. XI we examine the complete viscous equations to assess the validity of the viscous perturbation method for finite viscosity. Numerical examples are presented that indicate that instabilities may occur for certain ranges of Reynolds number. Finally, in Sec. XII experimental data for water at 15 GPa (Mineev and Zaidel', 1968) are discussed.

It is assumed that the shocked material behaves as a viscoelastic, Newtonian fluid. Anelastic absorption mechanisms are not explicitly considered, although they might be important in some experiments. The frequency of pressure waves generated by a perturbed shock are inversely proportional to the wavelength of the perturbation. For many materials it is therefore possible, at least in principle, to design an experiment that avoids anelastic phenomena.

II. BOUNDARY CONDITIONS AT THE SHOCK FRONT

The boundary conditions at the shock front are readily derived from the generalized Rankine-Hugoniot relations. Nevertheless, it seems worthwhile to derive these conditions because the result we obtain differs from that presented by Zaidel' (1967) without derivation. We begin the derivation by specifying the geometry at the shock front. This allows all perturbations to be cast into vector components normal and tangential to the shock front. These vector components are then used with the generalized Rankine-Hugoniot relations to obtain the boundary conditions at the shock front. Sign conventions follow Truesdell and Toupin (1960).

In following Zaidel' (1967) we adopt a comoving coordinate system (Fig. 4) in which the shock front is stationary, nominally the plane $x=0$. The shocked material travels in the positive x direction at a nominal velocity v ($v=U_S-U_P$, where U_S is the shock velocity and U_P is the particle velocity), and the unshocked material travels in the positive x direction at a nominal velocity v_0 (U_S). Perturbations are present in the x and y directions, but not in the z direction. The perturbations on the shock front ξ are positive when the front is perturbed toward the shocked material.

In the comoving coordinate system specified above (Fig. 4), a point on the shock front can be given by the generalized coordinate $(x,y)=(\xi(y),y)$, or in vector form by

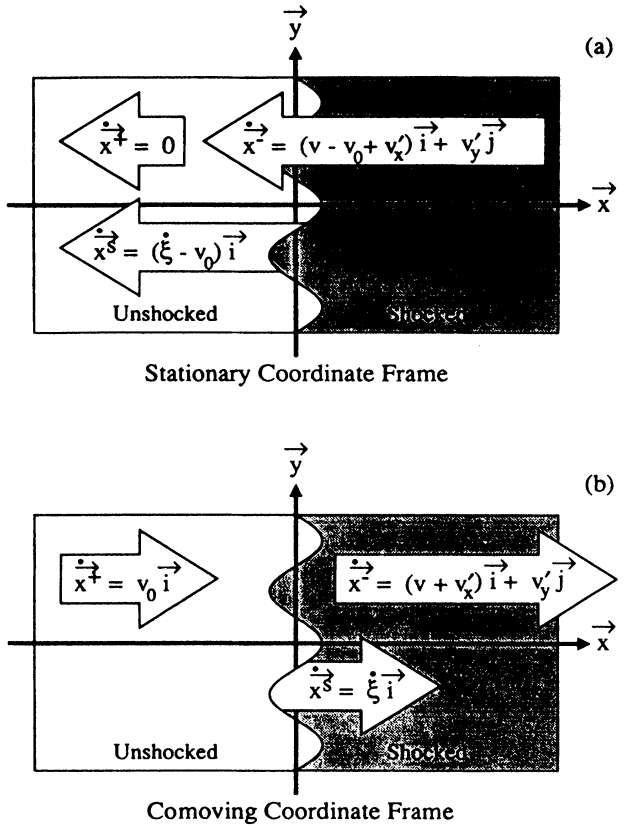

FIG. 4. Schematic geometry of sinusoidal perturbed shock (a) in stationary coordinate frame, and (b) in comoving coordinate frame. The arrows denote relative senses of motion, but their length is not scaled in proportion to the magnitudes of the velocities.

$$\vec{x}^S=\xi\vec{i}+y\vec{j}\ . \tag{1}$$

The tangent to this surface is given by $\partial\vec{x}^S/\partial y$. The normalized or unit tangent vector is then

$$\vec{t}=\frac{\xi_y\vec{i}+1\vec{j}}{\sqrt{1+\xi_y^2}}\ , \tag{2}$$

where $\xi_y\equiv\partial\xi/\partial y$, and the unit normal vector is given by

$$\vec{n}=\frac{1\vec{i}-\xi_y\vec{j}}{\sqrt{1+\xi_y^2}}\ . \tag{3}$$

The velocity of the surface point specified by Eq. (1) is

$$\dot{\vec{x}}^S=\dot{\xi}\vec{i}\ . \tag{4}$$

Its normal and tangential components are determined by the dot product of this velocity with the unit direction vector, Eqs. (2) and (3):

$$\dot{x}_n^S=\frac{\dot{\xi}}{\sqrt{1+\xi_y^2}} \tag{5}$$

and

$$\dot{x}_t^S=\frac{\xi_y\dot{\xi}}{\sqrt{1+\xi_y^2}}\ . \tag{6}$$

The unshocked material ahead of the shock wave is given by the generalized coordinate

$$\vec{x}^+=[x+v_0t]\vec{i}+y\vec{j} \tag{7}$$

with velocity

$$\dot{\vec{x}}^+=v_0\vec{i}\ . \tag{8}$$

This velocity can also be decomposed into normal and tangential components:

$$\dot{x}_n^+=\frac{v_0}{\sqrt{1+\xi_y^2}} \tag{9}$$

and

$$\dot{x}_t^+=\frac{\xi_y v_0}{\sqrt{1+\xi_y^2}}\ . \tag{10}$$

Similarly, the compressed material behind the shock front is given by the generalized coordinate

$$\vec{x}^-=[x+vt+v_x't]\vec{i}+[y+v_y't]\vec{j}\ , \tag{11}$$

where $v\vec{i}$ is the nominal velocity and primes denote small velocity perturbations $(v_x'\vec{i}+v_y'\vec{j})$. The velocity of the shocked material is

$$\dot{\vec{x}}^-=(v+v_x')\vec{i}+v_y'\vec{j}\ , \tag{12}$$

resolving into normal and tangential components

$$\dot{x}_n^-=\frac{v+v_x'-v_y'\xi_y}{\sqrt{1+\xi_y^2}}\ , \tag{13}$$

$$\dot{x}_t^-=\frac{v_y'+\xi_y(v+v_x')}{\sqrt{1+\xi_y^2}}\ . \tag{14}$$

In a reference frame moving with the shock front we define the normal velocities $U^{\pm}=\dot{x}_n^S-\dot{x}_n^{\pm}$

$$U^+=\frac{\dot{\xi}-v_0}{\sqrt{1+\xi_y^2}}\ , \tag{15}$$

$$U^-=\frac{\dot{\xi}-v-v_x'+v_y'\xi_y}{\sqrt{1+\xi_y^2}}\ . \tag{16}$$

Before evaluating the boundary conditions, it is useful to determine the components of the stress tensor in the (n,t) coordinate system. We assume a Newtonian fluid with constant viscosity. The stress tensor in the (x,y) coordinate frame is given by the components

$$\tau_{xx}=-P+\frac{2}{3}\eta\left[2\frac{\partial v_x}{\partial x}-\frac{\partial v_y}{\partial y}\right]+\kappa\left[\frac{\partial v_x}{\partial x}+\frac{\partial v_y}{\partial y}\right]\ , \tag{17}$$

$$\tau_{xy}=\tau_{yx}=\eta\left[\frac{\partial v_x}{\partial y}+\frac{\partial v_y}{\partial x}\right]\ , \tag{18}$$

$$\tau_{yy}=-P+\frac{2}{3}\eta\left[2\frac{\partial v_y}{\partial y}-\frac{\partial v_x}{\partial x}\right]+\kappa\left[\frac{\partial v_x}{\partial x}+\frac{\partial v_y}{\partial y}\right]\ , \tag{19}$$

where η is the shear viscosity. The bulk viscosity κ appears only in the diagonal elements τ_{ii}, i.e., those elements that describe compression without change in shape. These stress tensor components can be cast into normal and tangential stresses with the relationship

$$\tau_{kl}=\sum_i\sum_j(\vec{i}\cdot\vec{k})(\vec{j}\cdot\vec{l})\tau_{ij}\ . \tag{20}$$

Using the normal and tangent vectors determined above [Eqs. (2) and (3)] one can apply these sums to give

$$\tau_{nn}=\frac{\tau_{xx}-2\xi_y\tau_{xy}+\xi_y^2\tau_{yy}}{1+\xi_y^2}\ , \tag{21}$$

$$\tau_{nn}=-P+\kappa\left[\frac{\partial v_x}{\partial x}+\frac{\partial v_y}{\partial y}\right]+\frac{2}{3}\eta\frac{(2-\xi_y^2)\dfrac{\partial v_x'}{\partial x}-3\xi_y\left[\dfrac{\partial v_x'}{\partial y}+\dfrac{\partial v_y'}{\partial x}\right]+(2\xi_y^2-1)\dfrac{\partial v_y'}{\partial y}}{1+\xi_y^2}\ , \tag{22}$$

$$\tau_{nt}=\frac{\xi_y\tau_{xx}+(1-\xi_y^2)\tau_{xy}-\xi_y\tau_{yy}}{1+\xi_y^2}\ , \tag{23}$$

$$\tau_{nt}=\eta\frac{2\xi_y\dfrac{\partial v_x'}{\partial x}+(1-\xi_y^2)\left[\dfrac{\partial v_x'}{\partial y}+\dfrac{\partial v_y'}{\partial x}\right]-2\xi_y\dfrac{\partial v_y'}{\partial y}}{1+\xi_y^2} . \tag{24}$$

We now proceed to develop the boundary conditions. One boundary condition at the shock front is the Stokes-Christoffel condition, a conservation-of-mass equation (Truesdell and Toupin, 1960, pp. 519–523):

$$\rho^+U^+-\rho^-U^-\equiv[|\rho U|]=0 . \tag{25}$$

When we substitute the quantities determined above, this relation becomes

$$\rho_0(\dot\xi-v_0)=\rho(\dot\xi-v-v_x'+v_y'\xi_y) . \tag{26}$$

A second boundary condition at the shock front is Cauchy's first law of motion (Truesdell and Toupin, 1960, pp. 544–548), a stress balance, in the normal direction:

$$[|\tau_{nn}|]+\rho_0U^+[|\dot x_n|]=0 , \tag{27}$$

$$(P-P_0)(1+\xi_y^2)-\tfrac{2}{3}\eta\left[(2-\xi_y^2)\frac{\partial v_x'}{\partial x}-3\xi_y\left[\frac{\partial v_x'}{\partial y}+\frac{\partial v_y'}{\partial x}\right]+(2\xi_y^2-1)\frac{\partial v_y'}{\partial y}\right]$$
$$-\kappa(1+\xi_y^2)\left[\frac{\partial v_x}{\partial x}+\frac{\partial v_y}{\partial y}\right]+\rho_0(\dot\xi-v_0)(v_0-v-v_x'+v_y'\xi_y)=0 . \tag{28}$$

The third boundary condition derives from Cauchy's first law of motion in the tangential direction:

$$[|\tau_{nt}|]+\rho_0U^+[|\dot x_t|]=0 , \tag{29}$$

$$-\eta\left[2\xi_y\frac{\partial v_x'}{\partial x}+[1-\xi_y^2]\left[\frac{\partial v_x'}{\partial y}+\frac{\partial v_y'}{\partial x}\right]-2\xi_y\frac{\partial v_y'}{\partial y}\right]+\rho_0(\dot\xi-v_0)[\xi_yv_0-\xi_y(v+v_x')-v_y']=0 . \tag{30}$$

These boundary conditions can be linearized with the approximations

$$P\rightarrow P+P' , \tag{31}$$

and

$$\frac{1}{\rho}\rightarrow\frac{1}{\rho}-\frac{P'\delta}{\rho^2v^2} , \tag{32}$$

where

$$\delta\equiv-\rho_0^2v_0^2\frac{\partial V}{\partial P}\bigg|_{\text{Hugoniot}} \tag{33}$$

is a dimensionless measure of the compressibility on the Hugoniot, evaluated at the nominal shock pressure. Let all perturbations have the form e^{ik_0y}, i.e., suppose that the perturbations vary sinusoidally in the y direction, and collect terms of equal wave vector. Note that ξ, P', v_x', and v_y' are all perturbations of wave vector k_0. Terms of wave vector 0 (i.e., no perturbations) are

$$\rho_0v_0=\rho v \tag{34}$$

or

$$\rho=\rho_0\frac{U_S}{U_S-U_P} \tag{35}$$

from Eq. (26), and

$$P=P_0+\rho_0(v_0-v)v_0 , \tag{36}$$

or

$$P=P_0+\rho_0U_PU_S \tag{37}$$

from Eq. (28). Equation (30) gives no information with wave vector 0. Those terms that are first order in perturbations, i.e., with wave vector k_0, are

$$v_x'+\frac{P'\delta}{\rho v}-\left[\frac{\sigma-1}{\sigma}\right]\dot\xi=0 , \tag{38}$$

$$v_x'+\frac{P'}{\rho v}+\left[\frac{\sigma-1}{\sigma}\right]\dot\xi=\frac{2\nu}{3v}\left[2\frac{\partial v_x'}{\partial x}-\frac{\partial v_y'}{\partial y}\right]+\frac{\kappa}{\rho v}\left[\frac{\partial v_x'}{\partial x}+\frac{\partial v_y'}{\partial y}\right] , \tag{39}$$

$$v_y'-v(\sigma-1)\xi_y=\frac{\nu}{v}\left[\frac{\partial v_x'}{\partial y}+\frac{\partial v_y'}{\partial x}\right] , \tag{40}$$

where $\nu=\eta/\rho$ is the kinematic shear viscosity and

$$\sigma\equiv\frac{\rho}{\rho_0}=\frac{v_0}{v}>1 \tag{41}$$

is a measure of the strength of the shock. Writing ik_0v_x' for $\partial v_x'/\partial y$, making similar substitutions for $\partial v_y'/\partial y$ and ξ_y, and taking the Laplace transform, we find that the boundary conditions are then given by

$$\begin{bmatrix} \hat{v}_x \\ i\hat{v}_y \\ \hat{P}/(\rho v) \end{bmatrix}_{x=0} = \begin{bmatrix} -\frac{(\sigma-1)(1+\delta)}{\sigma(1-\delta)}(\xi_0 - s\hat{\xi}) - \frac{2\nu\delta}{3v(1-\delta)}\left[2\frac{\partial\hat{v}_x}{\partial x} - ik_0\hat{v}_y\right] - \frac{\kappa\delta}{\rho v(1-\delta)}\left[\frac{\partial\hat{v}_x}{\partial x} + ik_0\hat{v}_y\right] \\ -k_0 v(\sigma-1)\hat{\xi} + \frac{i\nu}{v}\left[ik_0\hat{v}_x + \frac{\partial\hat{v}_y}{\partial x}\right] \\ \frac{2(\sigma-1)}{\sigma(1-\delta)}(\xi_0 - s\hat{\xi}) + \frac{2\nu}{3v(1-\delta)}\left[2\frac{\partial\hat{v}_x}{\partial x} - ik_0\hat{v}_y\right] + \frac{\kappa}{\rho v(1-\delta)}\left[\frac{\partial\hat{v}_x}{\partial x} + ik_0\hat{v}_y\right] \end{bmatrix}_{x=0}, \quad (42)$$

where $\hat{f}(s)$ denotes the Laplace transform of $f(t)$.

In the limit of no viscosity, these boundary conditions reduce to those of Zaidel' (1967) [his Eq. (1.9)] and D'yakov (1954). When the viscous terms are retained, Eq. (40) is the same as Zaidel's Eq. (2.4a) (1967), but the other two viscous boundary conditions differ. Zaidel's boundary conditions may be written

$$\begin{bmatrix} \hat{v}_x \\ i\hat{v}_y \\ \hat{P}/(\rho v) \end{bmatrix}_{x=0} = \begin{bmatrix} -\frac{(\sigma-1)(1+\delta)}{\sigma(1-\delta)}(\xi_0 - s\hat{\xi}) - \frac{2\nu\beta^2}{3v(1-\beta^2)}\left[2\frac{\partial\hat{v}_x}{\partial x} - ik_0\hat{v}_y\right] \\ -k_0 v(\sigma-1)\hat{\xi} + \frac{i\nu}{v}\left[ik_0\hat{v}_x + \frac{\partial\hat{v}_y}{\partial x}\right] \\ \frac{2(\sigma-1)}{\sigma(1-\delta)}(\xi_0 - s\hat{\xi}) + \frac{2\nu}{3v(1-\beta^2)}\left[2\frac{\partial\hat{v}_x}{\partial x} - ik_0\hat{v}_y\right] \end{bmatrix}_{x=0}. \quad (43)$$

The bulk viscosity κ is neglected in Zaidel's analysis. The shear viscosity terms originating in the τ_{nn} component of the stress tensor differ from those of Eq. (42) by factors of $[\beta^2(1-\delta)]/[\delta(1-\beta^2)]$ for $\hat{v}_{x,x=0}$ and $(1-\delta)/(1-\beta^2)$ for $\hat{P}_{x=0}$. For water at 15 GPa these dimensionless factors are 1.03 and 1.01, respectively, thus the numerical consequences of these discrepancies are small in this case.

The jump conditions [Eqs. (25), (27), and (29)] strictly apply only when the shock front has no structure, i.e., the shock front is an abrupt discontinuity with no width. Lord Rayleigh (1910) demonstrated that a shock in a viscous material will necessarily have finite structure, thereby bringing into question the applicability of the jump relations. If the shock is planar, a steady, unchanging shock with finite width obeys the jump relations (Swan *et al.*, 1973) where the upstream (v^+, P^+) and downstream (v^-, P^-) properties are evaluated in the asymptotic limits $x \to \pm\infty$. Similarly, if the width of the shock front is sufficiently narrow compared to the radius of curvature of the shock ($r \approx 4\pi^2/k_0^2\xi$), then the jump conditions may be employed. This condition is readily satisfied in practice since the shock width is generally on the order of tens of nanometers in thickness (see, for example, Harris and Presles, 1981), decreasing with increasing shock pressure. A method for expressing the boundary conditions, given an approximation of the shock-front structure, is described by Istrakov and Librovich (1966).

III. INITIAL CONDITIONS—THEORY vs EXPERIMENT

The experiments of Sakharov *et al.* (1965) were designed to generate a perturbed shock wave while producing the least possible disturbance behind the shock front. Sakharov *et al.* (1965) state that the uniformity of the flow behind the shock is disturbed at distances of order ξ_0, the initial shock perturbation amplitude. To the extent that this was true, the approximate initial conditions,

$$v_x'(x,t=0) = v_y'(x,t=0) = P'(x,t=0) = 0, \quad (44)$$

are applicable everywhere except in the immediate vicinity of the shock front. These initial conditions, used by Zaidel' (1967), assume that the flow field is initially uniform everywhere behind the perturbed shock front.

These initial conditions are meant to be compatible with both the differential equations (derived below) and the boundary conditions. In fact, these initial conditions are not compatible with the boundary conditions, as can be seen by substituting Eq. (44) into Eq. (42). In the inviscid case $i\hat{v}_y = -k_0 v(\sigma-1)\hat{\xi}$; thus a finite shock-front perturbation, $\xi \neq 0$, is inconsistent with $\hat{v}_y = 0$ at the shock front $x = 0$. Zaidel' (1967) suggests that for the purpose of a stability analysis the initial conditions can be neglected. While this may be true, it remains to be shown that the initial conditions are unimportant for the purpose of modeling actual experiments.

The experimental realization of near-negligible initial velocity and pressure perturbations is difficult, since this also would create near-negligible shock-front disturbances that would be difficult to measure. It will be shown in Sec. V that the perturbation analysis is valid only in the limit $k_0\xi_0 \ll 1$. This, too, is difficult to realize experimentally, and in practice $k_0\xi_0$ was of order unity. Godunov *et al.* (1971) suggest that when $k_0\xi_0$ is large (of order unity), jetting may occur at the point where the initially planar shock first impinges on the corrugations. Godunov *et al.* (1969) observed such jets in experiments

where initially planar shocks met V-shaped grooves in metal targets. The implication is that the experimentally realized initial conditions may have been qualitatively very different from those supposed by the theory. The theory might be perfectly good, but not suited to the actual experimental conditions.

In Secs. V, VI, and VII, where we follow the derivation of Zaidel' (1967), the initial conditions will be neglected [i.e., we use Eq. (44)]. In Secs. IX and X the initial conditions will be reexamined and it will be shown that finite initial velocity and pressure perturbations do have a strong influence over the resulting shock-front perturbation development. Jetting in the corrugations is not included in our model.

IV. EQUATIONS OF MOTION AND CONTINUITY

The differential equations governing the compressible flow in the shocked sample are the standard equations of motion and continuity. For completeness, these equations will be presented and cast into the form used by Zaidel' (1967).

Noting that there is no z variation in any quantity, the equations of motion can be written as

$$\frac{\partial v_x}{\partial t}+v_x\frac{\partial v_x}{\partial x}+v_y\frac{\partial v_x}{\partial y}=\frac{1}{\rho}\left[\frac{\partial \tau_{xx}}{\partial x}+\frac{\partial \tau_{yx}}{\partial y}\right], \tag{45a}$$

$$\frac{\partial v_y}{\partial t}+v_x\frac{\partial v_y}{\partial x}+v_y\frac{\partial v_y}{\partial y}=\frac{1}{\rho}\left[\frac{\partial \tau_{xy}}{\partial x}+\frac{\partial \tau_{yy}}{\partial y}\right]. \tag{45b}$$

Next, we substitute the Newtonian viscosity form of the stress tensor [Eqs. (17), (18), and (19)] and linearize the equations. This linearization is accomplished by writing the velocities and pressure in terms of their nominal values plus a perturbation. Only those terms that are first order in the perturbations are retained. The perturbation quantities are denoted by primes:

$$v_x\rightarrow v+v_x', \tag{46}$$

$$v_y\rightarrow v_y', \tag{47}$$

$$P\rightarrow P+P'. \tag{48}$$

The resulting equations of motion are

$$\frac{\partial v_x'}{\partial t}+v\frac{\partial v_x'}{\partial x}+\frac{1}{\rho}\frac{\partial P'}{\partial x}=\nu\left[\frac{4}{3}\frac{\partial^2 v_x'}{\partial x^2}+\frac{\partial^2 v_x'}{\partial y^2}+\frac{1}{3}\frac{\partial^2 v_y'}{\partial x\partial y}\right]+\frac{\kappa}{\rho}\left[\frac{\partial^2 v_x'}{\partial x^2}+\frac{\partial^2 v_y'}{\partial x\partial y}\right], \tag{49a}$$

$$\frac{\partial v_y'}{\partial t}+v\frac{\partial v_y'}{\partial x}+\frac{1}{\rho}\frac{\partial P'}{\partial y}=\nu\left[\frac{1}{3}\frac{\partial^2 v_x'}{\partial x\partial y}+\frac{\partial^2 v_y'}{\partial x^2}+\frac{4}{3}\frac{\partial^2 v_y'}{\partial y^2}\right]+\frac{\kappa}{\rho}\left[\frac{\partial^2 v_x'}{\partial x\partial y}+\frac{\partial^2 v_y'}{\partial y^2}\right]. \tag{49b}$$

The equation of continuity is

$$\frac{\partial \rho}{\partial t}+\frac{\partial}{\partial x}(\rho v_x)+\frac{\partial}{\partial y}(\rho v_y)=0. \tag{50}$$

This equation is linearized with the adiabatic approximation:

$$\frac{1}{\rho}\rightarrow\frac{1}{\rho}-\frac{P'}{\rho^2 c^2}, \tag{51}$$

resulting in the equation

$$\frac{\partial P'}{\partial t}+v\frac{\partial P'}{\partial x}+\rho c^2\left[\frac{\partial v_x'}{\partial x}+\frac{\partial v_y'}{\partial y}\right]=0. \tag{52}$$

The complete differential equations [(49a), (49b), and (52)] are solvable in principle. The algebraic complexity of the system is formidable, however, so a perturbation method is adopted. First the equations are solved in the inviscid limit. The role of viscosity is then examined by considering viscous effects to be the result of small perturbations on the inviscid solution. The complete equations will be readdresed in Sec. XI.

Dropping the primes on the perturbed quantities in the linearized equations of motion and continuity, taking their Laplace transform, and letting all perturbed quantities depend on y as $e^{ik_0 y}$, we can express these equations in matrix form,

$$\frac{\partial \vec{u}}{\partial x}=\mathbf{A}\vec{u}+\vec{g}, \tag{53a}$$

where

$$\vec{u}\equiv\begin{bmatrix}\hat{v}_x\\ i\hat{v}_y\\ \hat{P}/(\rho v)\end{bmatrix}, \tag{53b}$$

$$\mathbf{A}\equiv\begin{bmatrix}\frac{\beta^2 k_0 z}{1-\beta^2} & \frac{-k_0}{1-\beta^2} & \frac{-\beta^2 k_0 z}{1-\beta^2}\\ 0 & -k_0 z & k_0\\ \frac{-k_0 z}{1-\beta^2} & \frac{k_0}{1-\beta^2} & \frac{\beta^2 k_0 z}{1-\beta^2}\end{bmatrix} \tag{53c}$$

and

$$\vec{g}\equiv\begin{bmatrix}\frac{\beta^2}{v(1-\beta^2)}\left[\frac{P(0)}{\rho v}-v_x(0)\right]\\ \frac{iv_y(0)}{v}\\ \frac{1}{v(1-\beta^2)}\left[v_x(0)-\beta^2\frac{P(0)}{\rho v}\right]\end{bmatrix}+\begin{bmatrix}-\frac{\beta^2}{v(1-\beta^2)}\left[\nu\left[\frac{4}{3}\frac{\partial^2\hat{v}_x}{\partial x^2}-k_0^2\hat{v}_x+\frac{ik_0}{3}\frac{\partial\hat{v}_y}{\partial x}\right]+\frac{\kappa}{\rho}\left[\frac{\partial^2\hat{v}_x}{\partial x^2}+ik_0\frac{\partial\hat{v}_y}{\partial x}\right]\right]\\ \frac{i}{v}\left[\nu\left[\frac{ik_0}{3}\frac{\partial\hat{v}_x}{\partial x}+\frac{\partial^2\hat{v}_y}{\partial x^2}-\frac{4k_0^2}{3}\hat{v}_y\right]+\frac{\kappa}{\rho}\left[ik_0\frac{\partial\hat{v}_x}{\partial x}-k_0^2\hat{v}_y\right]\right]\\ \frac{1}{v(1-\beta^2)}\left[\nu\left[\frac{4}{3}\frac{\partial^2\hat{v}_x}{\partial x^2}-k_0^2\hat{v}_x+\frac{ik_0}{3}\frac{\partial\hat{v}_y}{\partial x}\right]+\frac{\kappa}{\rho}\left[\frac{\partial^2\hat{v}_x}{\partial x^2}+ik_0\frac{\partial\hat{v}_y}{\partial x}\right]\right]\end{bmatrix}. \tag{53d}$$

The factor e^{ik_0y} has been omitted for clarity.

$$\beta \equiv \frac{v}{c} \tag{54}$$

is the Mach number of the shocked sample with respect to the high-pressure sound speed c, and

$$z \equiv \frac{s}{k_0 v} \tag{55}$$

is a dimensionless form of the Laplace transform variable s.

Supposing that the inviscid solution of Eq. (53) has the form

$$\vec{u} = \vec{u}_{x=0} e^{\lambda x} \tag{56}$$

leads to a characteristic equation for the eigenvalues λ. From the characteristic equation we get three eigenvalues and three corresponding left eigenvectors ($\Psi \mathbf{A} = \lambda \Psi$):

$$\lambda_1 = -k_0 z \ , \quad \lambda_2 = \frac{k_0(\beta^2 z - \omega)}{1-\beta^2} \ , \quad \lambda_3 = \frac{k_0(\beta^2 z + \omega)}{1-\beta^2} \ , \tag{57}$$

$$\Psi_1 = \begin{bmatrix} -1 \\ z \\ -1 \end{bmatrix}^t \ , \quad \Psi_2 = \begin{bmatrix} z \\ -1 \\ \omega \end{bmatrix}^t \ , \quad \Psi_3 = \begin{bmatrix} z \\ -1 \\ -\omega \end{bmatrix}^t \ , \tag{58}$$

where

$$\omega \equiv \sqrt{\beta^2 z^2 + 1 - \beta^2} \ . \tag{59}$$

It is convenient to decompose the matrix of Eq. (53) into the form

$$\mathbf{A} = \mathbf{S}^{-1} \mathbf{\Lambda} \mathbf{S} \ , \tag{60}$$

where $\mathbf{S}$ is the matrix whose rows are the left eigenvectors and Λ is the diagonal matrix of eigenvalues:

$$\begin{bmatrix} \frac{\beta^2 k_0 z}{1-\beta^2} & \frac{-k_0}{1-\beta^2} & \frac{-\beta^2 k_0 z}{1-\beta^2} \\ 0 & -k_0 z & k_0 \\ \frac{-k_0 z}{1-\beta^2} & \frac{k_0}{1-\beta^2} & \frac{\beta^2 k_0 z}{1-\beta^2} \end{bmatrix}$$

$$= \begin{bmatrix} \frac{1}{z^2-1} & \frac{\omega z+1}{2\omega(z^2-1)} & \frac{\omega z-1}{2\omega(z^2-1)} \\ \frac{z}{z^2-1} & \frac{\omega+z}{2\omega(z^2-1)} & \frac{\omega-z}{2\omega(z^2-1)} \\ 0 & \frac{1}{2\omega} & \frac{-1}{2\omega} \end{bmatrix} \begin{bmatrix} -zk_0 & 0 & 0 \\ 0 & \frac{k_0(\beta^2 z-\omega)}{1-\beta^2} & 0 \\ 0 & 0 & \frac{k_0(\beta^2 z+\omega)}{1-\beta^2} \end{bmatrix} \begin{bmatrix} -1 & z & -1 \\ z & -1 & \omega \\ z & -1 & -\omega \end{bmatrix} . \tag{61}$$

The differential equations (53) can then be solved as

$$\frac{\partial}{\partial x} \vec{u} = \mathbf{S}^{-1} \mathbf{\Lambda} \mathbf{S} \vec{u} + \vec{g} \ , \tag{62}$$

$$\frac{\partial}{\partial x} (\mathbf{S}\vec{u}) = \mathbf{\Lambda}(\mathbf{S}\vec{u}) + (\mathbf{S}\vec{g}) \ , \tag{63}$$

$$(\mathbf{S}\vec{u}) = e^{\Lambda x} \left[(\mathbf{S}\vec{u})_{x=0} + \int_0^x e^{-\Lambda \chi} (\mathbf{S}\vec{g}) \partial \chi \right] , \tag{64}$$

$$\vec{u} = \mathbf{S}^{-1} e^{\Lambda x} \left[(\mathbf{S}\vec{u})_{x=0} + \int_0^x e^{-\Lambda \chi} (\mathbf{S}\vec{g}) \partial \chi \right] , \tag{65}$$

when the viscous terms in $\vec{g}$ and $\vec{u}_{x=0}$ are considered as small perturbations.

V. SOLUTION IN THE INVISCID LIMIT

Note that there are three boundary conditions that determine the solution $\vec{u}$ for an arbitrary forcing function $\hat{\xi}$. Since we are interested in determining this function, we require an additional constraint. The approach that Zaidel' (1967) adopted was to consider the long-time behavior of the solution. If one requires all quantities to be bounded, λ must be negative for some real positive s. λ_3 violates this constraint. The solution is therefore given by setting the third component of the vector $\mathbf{S}\vec{u}$, the coefficient of λ_3, equal to zero. In a real experiment, there may be some boundary at a finite distance from the shock front where perturbations must go to zero. Such a boundary could be a driver plate-sample interface, for example. A finite boundary condition of this type would allow all three eigenvectors to participate in the solution, although the contribution of the third would have to approach zero as the boundary moves farther from the shock front.

Adopting this approximation we can write

$$(\mathbf{S}\vec{u})_{x=0}=\begin{bmatrix} -\frac{\sigma-1}{\sigma}[k_0 v\hat{\xi}(\sigma-1)z+\xi_0] \\ \frac{\sigma-1}{\sigma(1-\delta)}\{k_0 v\hat{\xi}[(1+\delta)z^2-2\omega z+\sigma(1-\delta)]-\xi_0[(1+\delta)z-2\omega]\} \\ \frac{\sigma-1}{\sigma(1-\delta)}\{k_0 v\hat{\xi}[(1+\delta)z^2+2\omega z+\sigma(1-\delta)]-\xi_0[(1+\delta)z+2\omega]\} \end{bmatrix} \tag{66}$$

by multiplying the vector of boundary conditions, $\vec{u}_{x=0}$ [Eq. (41)] in the inviscid limit, by the matrix **S** given in Eq. (61). The initial condition contribution to Eq. (65) is given by

$$\int_0^x \partial\chi e^{-\Lambda\chi}(\mathbf{S}\vec{g})=\int_0^x \partial\chi \begin{bmatrix} e^{-\lambda_1\chi}\frac{iv_y(0)-v_x(0)}{v} \\ e^{-\lambda_2\chi}\frac{\beta^2(z-\omega)\left[\frac{P(0)}{\rho v}\right]-(\beta^2 z-\omega)v_x(0)-i(1-\beta^2)v_y(0)}{v(1-\beta^2)} \\ e^{-\lambda_3\chi}\frac{\beta^2(z+\omega)\left[\frac{P(0)}{\rho v}\right]-(\beta^2 z+\omega)v_x(0)-i(1-\beta^2)v_y(0)}{v(1-\beta^2)} \end{bmatrix} . \tag{67}$$

In the limit $x\to\infty$ we require all perturbations to vanish, and the solution is therefore determined by setting the sum of the third components of the vectors given by Eqs. (66) and (67) to zero. The dimensionless amplitude of the shock-front corrugation, $\phi\equiv\xi/\xi_0$, can then be written as

$$\hat{\phi}\equiv\frac{\hat{\xi}}{\xi_0}=\frac{1}{k_0 v}\frac{(1+\delta)z+2\omega}{(1+\delta)z^2+2\omega z+\sigma(1-\delta)} \tag{68a}$$

$$-\frac{1}{k_0 v}\frac{\sigma(1-\delta)}{\xi_0(\sigma-1)v(1-\beta^2)}\frac{\int_0^\infty \partial\chi e^{-\lambda_3\chi}\left[\beta^2(z+\omega)\left[\frac{P(0)}{\rho v}\right]-(\beta^2 z+\omega)v_x(0)-i(1-\beta^2)v_y(0)\right]}{(1+\delta)z^2+2\omega z+\sigma(1-\delta)} . \tag{68b}$$

Zaidel' (1967) noted that the second term containing the initial conditions will always be finite. He reasoned that it is therefore sufficient, for the purpose of a stability analysis, to neglect this term [i.e., use the initial conditions of Eq. (44)]. This is reasonable, but may be insufficient for the modeling of real experiments. For the purpose of reproducing his results, we shall accept this approximation for now. The initial conditions will be reexamined in Sec. IX.

To invert Eq. (68a), it is convenient to transform variables according to

$$\epsilon\equiv\frac{1-\beta^2}{\beta^2} , \tag{69}$$

$$\mu\equiv\sqrt{\epsilon} , \tag{70}$$

$$T\equiv\mu\tau=k_0 ct\sqrt{1-\beta^2}=k_0 v\mu t , \tag{71}$$

$$z=\frac{\mu}{2}\left[W-\frac{1}{W}\right] , \tag{72}$$

$$\omega=\frac{\beta\mu}{2}\left[W+\frac{1}{W}\right] , \tag{73}$$

to give the result

$$\phi\equiv\frac{\xi}{\xi_0}=\frac{1}{2\pi i}\int \exp\left[\frac{1}{2}T\left[W-\frac{1}{W}\right]\right]dW\left[W+\frac{1}{W}\right]\frac{W^2(1+\delta+2\beta)-(1+\delta-2\beta)}{W^4(1+\delta+2\beta)+W^2\left[\frac{4\sigma}{\epsilon}(1-\delta)-2(1+\delta)\right]+(1+\delta-2\beta)} . \tag{74}$$

This expression is similar to Zaidel's (1967) Eqs. (1.16) and (1.17) (he is missing the term $W+1/W$, probably a typographic error).

With this transformation, the branch $+\sqrt{\beta^2 z^2+1-\beta^2}$ in the complex z plane is mapped onto the right half of the complex W plane ($\mathrm{Re}[W]>0$). On this half-plane, $\mathrm{Re}[z]$ will be negative when $|W|<1$ and positive when $|W|>1$. If the poles of Eq. (74) lie outside the unit circle, $|W|=1$, then a pole in the z plane will exist with $\mathrm{Re}[z]>0$, and the solution will consequently be unbounded as $t\rightarrow\infty$. It is easily shown that all singularities of the integrand lie within the unit circle $|W|=1$ when

$$\frac{\sigma-\epsilon}{\sigma+\epsilon}<\delta<1 . \tag{75}$$

When these inequalities are satisfied, the solution will be bounded and the shock will be stable. These inequalities are identical to Kontorovich's (1957) requirements for the stability of a shock wave [correcting D'yakov's (1954) earlier work]. The inequality $\delta<1$ is satisfied when the shock velocity increases with increasing particle velocity, $\partial U_S/\partial U_P>0$. The second inequality, $\delta>(\sigma-\epsilon)/(\sigma+\epsilon)$, is satisfied when the high-pressure isentropic bulk modulus K_S is greater than both $(P-P_0)/(\sigma-1)$ and $(P-P_0)(1+\gamma)$, assuming γ, the thermodynamic Grüneisen parameter, is less than $2/(\sigma-1)$. A discussion of the relationship between these stability criteria and the conditions for shock splitting is given by Fowles and Houwing (1984).

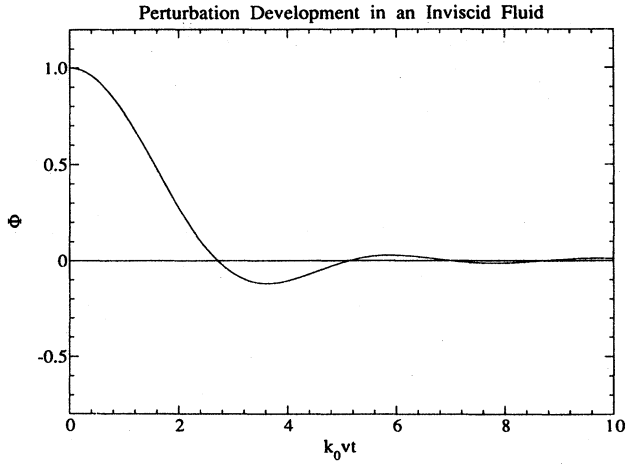

FIG. 5. Development of corrugated shock perturbations in an inviscid fluid. Calculated with Eq. (79) with the parameters listed in Table I.

Assuming the singularities lie within the unit circle, we can let the contour of integration be a counterclockwise unit circle:

$$W=e^{2\pi i y} , \tag{76}$$

$$\phi=2\int_0^1 e^{iT\sin(2\pi y)}dy\,\cos(2\pi y)\frac{e^{6\pi i y}(1+\delta+2\beta)-e^{2\pi i y}(1+\delta-2\beta)}{e^{8\pi i y}(1+\delta+2\beta)+e^{4\pi i y}\left[\frac{4\sigma}{\epsilon}(1-\delta)-2(1+\delta)\right]+(1+\delta-2\beta)} . \tag{77}$$

Multiplying through by the complex conjugate of the denominator, making another change of variables,

$$X=\sin(2\pi y) , \tag{78}$$

and using symmetry to eliminate terms gives

$$\phi=\frac{4\beta\epsilon\sigma(1-\delta)}{\pi}\int_0^1\frac{\cos(TX)\sqrt{1-X^2}\,\partial X}{\epsilon^2X^4[(1+\delta)^2-4\beta^2]+2\epsilon X^2[2(1-\beta^2)-\sigma(1-\delta^2)]+\sigma^2(1-\delta)^2} . \tag{79}$$

This is the final expression for the amplitude of the shock-front perturbation in the inviscid limit when the initial conditions are neglected (Fig. 5). Note that the initial time derivative of Eq. (79), $\dot{\phi}_0$, is zero [$\dot{\phi}$ is a function of $\sin(TX)$, which is zero at $T=0$]. This result is similar to Zaidel's (1967) Eqs. (1.20) and (1.21), but he is missing the $4\beta^2$ term in the denominator (probably a typographic error).

By substituting the solution, Eq. (68a), into the boundary conditions, Eq. (42), we can solve Eq. (65) for the inviscid velocity and pressure perturbations:

$$\hat{v}_x=\frac{\xi_0(\sigma-1)}{1-z^2}\frac{[(1+\delta)z^2+2\omega z+(1-\delta)]e^{\lambda_1 x}-2(1+\omega z)e^{\lambda_2 x}}{(1+\delta)z^2+2\omega z+\sigma(1-\delta)} , \tag{80a}$$

$$i\hat{v}_y=\frac{\xi_0(\sigma-1)}{1-z^2}\frac{z[(1+\delta)z^2+2\omega z+(1-\delta)]e^{\lambda_1 x}-2(\omega+z)e^{\lambda_2 x}}{(1+\delta)z^2+2\omega z+\sigma(1-\delta)} , \tag{80b}$$

$$\frac{\hat{P}}{\rho v}=2\xi_0(\sigma-1)\frac{e^{\lambda_2 x}}{(1+\delta)z^2+2\omega z+\sigma(1-\delta)} . \tag{80c}$$

TABLE I. Water parameters at 15 GPa to model Mineev and Zaidel' (1968).

Parameter	Eq.	Value
v_0		5.383 km/s
v		3.140 km/s
c		5.8 km/s
σ	(42)	1.714
β	(54)	0.541
δ	(136)	0.287
ϵ	(69)	1.153
μ	(70)	1.074
k_0		2π cm^{-1}
$k_0\xi_0$		1
α	(109)	0.056
S	(111)	−0.47

D'yakov (1954) found that a perturbed shock front generates two types of motion. The first type, in which entropy changes while pressure remains constant, he calls entropy-vortex waves. This motion is related to the eigenvalue λ_1. The second type of motion, in which entropy is constant while pressure changes, is sound waves. The eigenvalues λ_2 and λ_3 are related to these waves.

The existence of the two wave types suggests competing roles for the bulk and shear viscosities. Incompressible flow, entropy-vortex waves in this case, is independent of the bulk viscosity. Sound waves, in which compression does occur, are dependent on both the shear and the bulk viscosities (see, for example, Landau and Lifshitz, 1959, pp. 298–302).

The velocity and pressure perturbations for an inviscid fluid are plotted in Figs. 6(a) and 6(b). The initially large tangential velocities induced by the perturbed shock generate pronounced vortices that are advected away from shock front with time. Lesser vortices are generated as velocities at the shock front fluctuate with time. Where the perturbed shock lags behind its nominal position, that is, $\phi>0$, positive pressure perturbations build up behind the front, thereby accelerating the shock. Later, when the shock leads it nominal position, that is, $\phi<0$, negative pressure perturbations develop that decelerate the shock. Pressure-driven (acoustic) velocity perturbations propagate the energy of this oscillatory system away from the shock front, causing the shock amplitude oscillations to decay with time.

Note that the peak pressure perturbations are of the order $k_0\xi_0\rho v^2=k_0\xi_0(\sigma-1)P_{\text{Hugoniot}}$ [Fig. 6(b)]. When the product $k_0\xi_0$ is of order unity, pressure perturbations will be nearly as large as the nominal Hugoniot pressure. The linearizing approximations [Eqs. (32) and (51)] are valid only in the limit $P'\to 0$; thus this theory is applicable only when the amplitude of the shock perturbations is much less than the wavelength of the perturbations, $k_0\xi_0\ll 1$.

For future reference, note that when the transformations (69)–(73), (76), and (78) are applicable, a single transformation can be employed:

$$z\to i\mu X\ , \tag{81a}$$

$$\omega\to\mu\beta\sqrt{1-X^2}\ . \tag{81b}$$

VI. VISCOUS PERTURBATIONS

The essence of the perturbation treatment is to evaluate the viscous stresses given the inviscid solution. The method of solution follows from Eqs. (62)–(65), but now the viscous terms in the boundary conditions, $\mathbf{u}_{x=0}$, and the vector $\mathbf{g}$ are evaluated from the inviscid solution, Eq. (80). Now, as before, we require the solution to be finite for all values of x. Since the third eigenvalue leads to exponential growth of the perturbations, the part of the solution [Eq. (64)] that is weighted by this eigenvalue must be identically zero. This constraint gives the result

$$k_0 v\hat{\phi}=\frac{(1+\delta)z+2\omega}{(1+\delta)z^2+2\omega z+\sigma(1-\delta)} \tag{82a}$$

$$+\frac{\sigma}{R_s}\frac{z^2[(1+\delta)^2+4\beta^2]+4\omega z(1+\delta)+[4(2-\beta^2)-(1+\delta)^2]}{[(1+\delta)z^2+2\omega z+\sigma(1-\delta)]^2} \tag{82b}$$

$$-\frac{2\sigma}{\epsilon R_b}\frac{(z-\omega)(\delta z+\omega)}{[(1+\delta)z^2+2\omega z+\sigma(1-\delta)]^2} \tag{82c}$$

$$-\frac{\sigma(1-\delta)}{R_s}\frac{z^2(1+\delta)+2\omega z+(1-\delta)}{[(1+\delta)z^2+2\omega z+\sigma(1-\delta)]^2} \tag{82d}$$

$$+\frac{\sigma(1-\delta)}{\epsilon R_b}\frac{(z-\omega)(\omega^2+1)}{\omega[(1+\delta)z^2+2\omega z+\sigma(1-\delta)]^2}\ , \tag{82e}$$

where the shear Reynolds number is defined as

$$R_s\equiv\frac{v}{k_0\nu}=\frac{v\rho}{k_0\eta} \tag{83}$$

and, by analogy, the bulk Reynolds number is defined as

$$R_b\equiv\frac{v\rho}{k_0(\frac{4}{3}\eta+\kappa)}\ . \tag{84}$$

The first term [Eq. (82a)] is the Laplace transform of the inviscid solution, and the remaining terms are the viscous perturbations. Equations (82b) and (82c) arise

from the surface (i.e., the boundary conditions), and Eqs. (82d) and (82e) arise from the volume of the shocked fluid.

Since the poles of Eqs. (82b), (82c), and (82d) are identical to those of the inviscid solution, Eq. (82a), the transformations of Eq. (81) can be applied in the inverse Laplace transformation of these terms. The ω in the denominator of Eq. (82e) introduces a singularity at the branch point $W=\pm i$; thus the transformation, Eq. (81), alone is not applicable for the inversion of this term. To invert this term we use the convolution theorem:

$$\frac{1}{\omega}\hat{f}(z)\rightarrow\frac{1}{\beta\mu}\int_0^T \partial u\, f(u)J_0(T-u)\,, \tag{85}$$

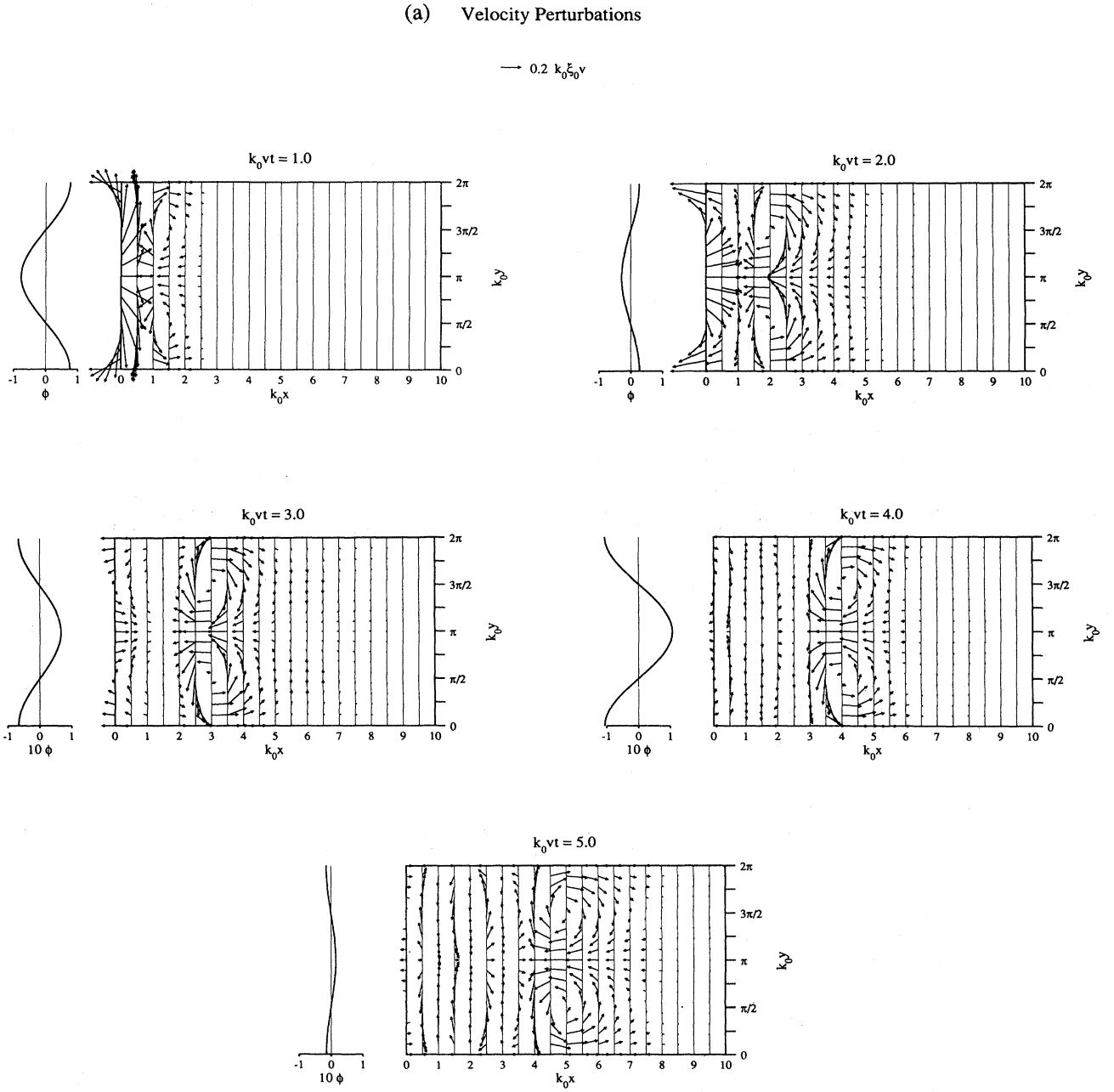

FIG. 6. Perturbation velocities and pressure at various times corresponding to Fig. 5. These perturbations were calculated numerically from Eq. (80) with the twentieth-order shifted Lagrange polynomial quadrature method of Bellman *et al.* (1966). The magnitude of the velocity perturbations is proportional to the length of the arrows or line segments, and the magnitude of pressure perturbations is proportional to the diameter of the circles. The normalized shock-perturbation amplitude is plotted offset to the left of the figures for clarity.

(b) Pressure Perturbations

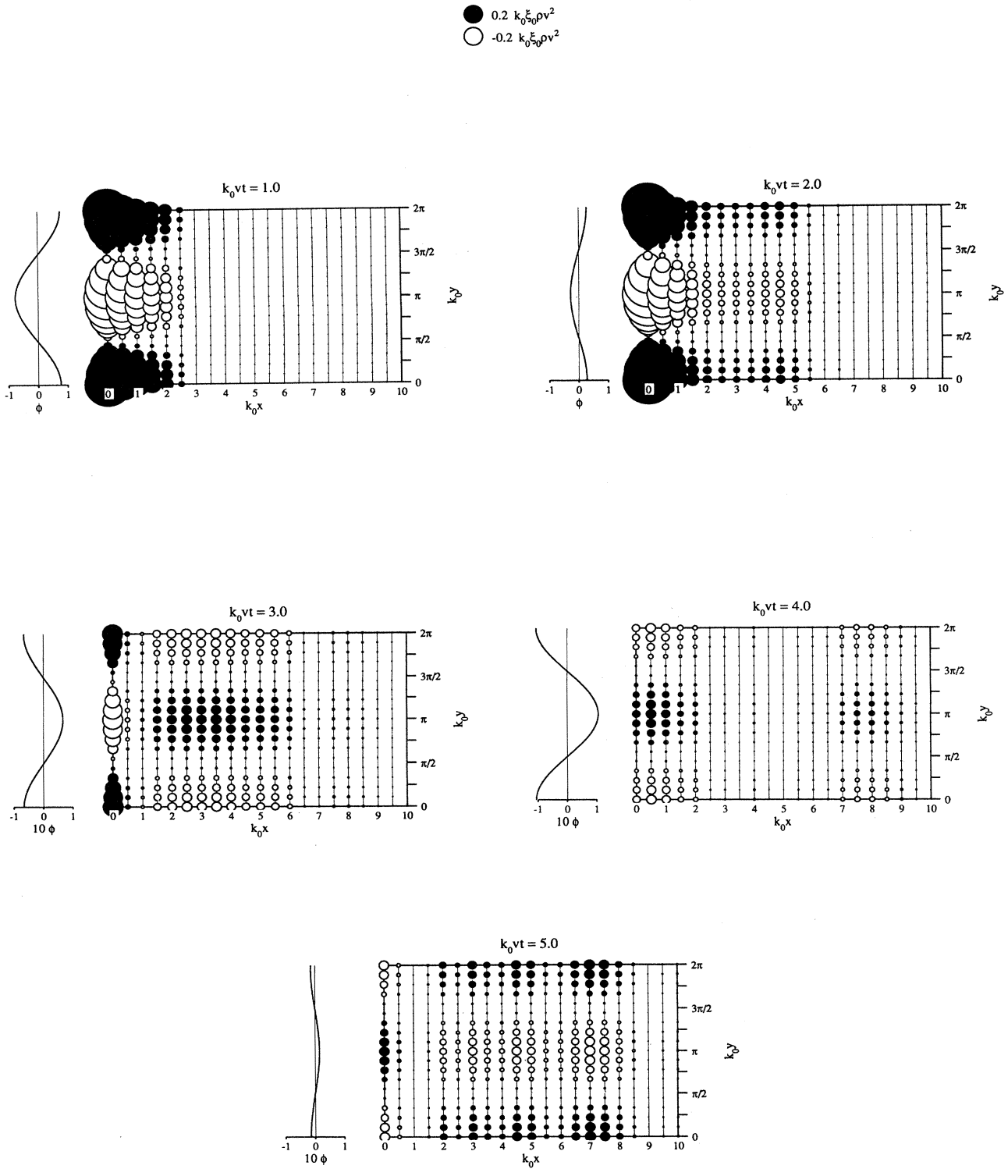

FIG. 6. (*Continued*).

$$\phi = \frac{4\beta\epsilon\sigma(1-\delta)}{\pi}\int_0^1 \partial X \frac{\cos(TX)\sqrt{1-X^2}}{\epsilon^2 X^4[(1+\delta)^2-4\beta^2]+2\epsilon X^2[2(1-\beta^2)-\sigma(1-\delta^2)]+\sigma^2(1-\delta)^2} \tag{86a}$$

$$+\frac{4\sigma\beta u}{\pi R_b}\int_0^1 \partial X\, X\sqrt{1-X^2}\sin(TX)\frac{\epsilon^2X^4[8\beta^2+(1+\delta)(1-4\delta-\delta^2)]-2\epsilon X^2\{4(1-\beta^2)+\sigma[2(1+\beta^2)-(1+\delta)^2]\}+\sigma(1-\delta)[4(1-\beta^2)+\sigma(1-\delta)^2]}{\{\epsilon^2X^4[(1+\delta)^2-4\beta^2]+2\epsilon X^2[2(1-\beta^2)-\sigma(1-\delta^2)]+\sigma^2(1-\delta)^2\}^2} \tag{86b}$$

$$-\frac{8\sigma\beta u\epsilon(1-\delta)}{3\pi R_s}\int_0^1 \partial X\, X\sqrt{1-X^2}\sin(TX)\frac{\epsilon X^2\{(3+\delta)(1+\delta)-\sigma[(1+\delta)^2-4\beta^2]\}-\sigma[4(2-\beta^2)-(1+\delta)^2-\sigma(1-\delta^2)]}{\{\epsilon^2X^4[(1+\delta)^2-4\beta^2]+2\epsilon X^2[2(1-\beta^2)-\sigma(1-\delta^2)]+\sigma^2(1-\delta)^2\}^2} \tag{86c}$$

$$-\frac{2\sigma\beta u(1-\delta)}{\pi R_b}\int_0^1 \partial X\, X\sqrt{1-X^2}\sin(TX)\frac{\epsilon^2X^4[(1+\delta)^2+4\beta^2(2+\delta)]-2\epsilon X^2[2(3+2\delta)-2\beta^2(2+\delta)+\sigma(1-\delta)(1+\delta+2\beta^2)]+\sigma(1-\delta)[8-4\beta^2+\sigma(1-\delta)]}{\{\epsilon^2X^4[(1+\delta)^2-4\beta^2]+2\epsilon X^2[2(1-\beta^2)-\sigma(1-\delta^2)]+\sigma^2(1-\delta)^2\}^2} \tag{86d}$$

$$-\frac{8\sigma(1-\delta)}{\pi R_b}\int_0^1 \partial X\, X^2\sqrt{1-X^2}\Xi_C(T,X)\frac{\epsilon X^2(1+\delta)-\sigma(1-\delta)}{\{\epsilon^2X^4[(1+\delta)^2-4\beta^2)]+2\epsilon X^2[2(1-\beta^2)-\sigma(1-\delta)^2]+\sigma^2(1-\delta)^2\}^2} \tag{86e}$$

$$-\frac{12\sigma\beta u\epsilon(1-\delta)}{3\pi R_s}\int_0^1 \partial X\, X\sqrt{1-X^2}\sin(TX)\frac{\epsilon^2X^4[(1+\delta)^2-4\beta^2]+2\epsilon X^2(1+\delta^2-2\beta^2)+\sigma(2-\sigma)(1-\delta)^2}{\{\epsilon^2X^4[(1+\delta)^2-4\beta^2)]+2\epsilon X^2[2(1-\beta^2)-\sigma(1-\delta)^2]+\sigma^2(1-\delta)^2\}^2}\,. \tag{86f}$$

where $J_0(T)$ is the zero-order Bessel function of the first kind.

The complete viscous solution may then be written as in Eqs. (86a)–(86f), where

$$\Xi_C(T,X)\equiv\int_0^T \partial u\,\cos(uX)J_0(T-u)\,. \tag{87}$$

Equation (86a) is the inviscid solution, Eqs. (86b) and (86c) are viscous terms that arise from the boundary conditions, and Eqs. (86d), (86e), and (86f) are viscous terms that arise from the volume (Fig. 7). Those terms containing R_b have their origin in sound waves, while those viscous terms independent of R_b originate from the entropy-vortex waves.

This result differs significantly from that given by Zaidel's (1967) Eq. (2.8). This is not surprising, however, considering that our boundary conditions differ. Using his boundary conditions, however, we also arrive at a

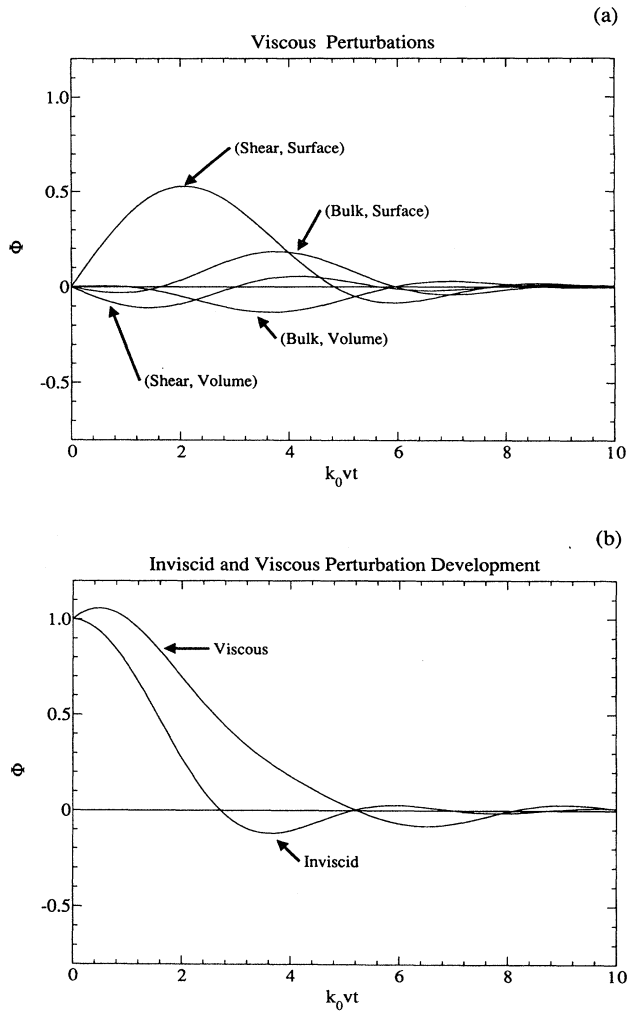

FIG. 7. Viscous perturbations. (a) Shear and bulk perturbations from surface and volume sources [Eq. (86)] and (b) shock corrugations amplitude for $R_s=4.23$ and $\kappa=\eta$ calculated with perturbation method [Eq. (86)] compared to inviscid solution [Eq. (79)] for parameters listed in Table I.

different result than he presents. The solution obtained from his boundary conditions is presented in the following section.

The initial slopes of the viscous perturbations can be determined from

$$\lim_{t\to 0}\dot{\hat{\phi}}=\lim_{\omega\to\beta z,\ z\to\infty}(k_0 v z)^2\hat{\phi}$$
$$=\frac{2k_0v\sigma(\beta+\delta)}{R_s(1+\delta+2\beta)}-\frac{k_0v\sigma(1-\beta)[\beta(1+\delta)+2\delta]}{R_b\epsilon(1+\delta+2\beta)^2}\ , \tag{88}$$

where we use the fact that the initial value of the viscous perturbations is zero. For all well behaved systems, i.e., $\delta>0$, that part of the solution dependent on shear viscosity has a positive initial slope. Conversely, the bulk viscosity contribution is initially negative. This limit predicts, therefore, that shear viscosity will initially amplify the shock perturbations rather than dampen them. That this is contrary to the behavior reported by Sakharov *et al.*, (1965) may indicate the importance of the bulk viscosity in their experiments.

VII. VISCOUS PERTURBATION WITH THE BOUNDARY CONDITIONS OF ZAIDEL' (1967)

For the purpose of comparison with Zaidel' (1967), we shall derive the viscous perturbation term from the boundary conditions that he proposes. His boundary conditions [his Eq. (2.4)] are given by Eq. (43) and neglect the bulk viscosity. Using these boundary conditions, and solving for the shock perturbation amplitude as before, we obtain the solution

$$k_0v\hat{\phi}=\frac{(1+\delta)z+2\omega}{(1+\delta)z^2+2\omega z+\sigma(1-\delta)} \tag{89a}$$
$$+\frac{\sigma(1-\delta)}{3R_s(1-\beta^2)}\frac{z^2[12\beta^2+3(1+\beta^2)(1+\delta)]+2\omega z[(3-\beta^2)+3(1+\delta)]+[8+13(1-\beta^2)+3\delta(1-\beta^2)]}{[(1+\delta)z^2+2\omega z+\sigma(1-\delta)]^2} \tag{89b}$$
$$+\frac{\sigma(1-\delta)}{3R_s(1-\beta^2)}\frac{4\beta^2(z-\omega)(\omega^2+1)-3\omega(1-\beta^2)[z^2(1+\delta)+2\omega z+(1-\delta)]}{\omega[(1+\delta)z^2+2\omega z+\sigma(1-\delta)]^2}\ , \tag{89c}$$

again breaking up into the inviscid component, Eq. (89a), and viscous perturbations, Eqs. (89b) and (89c). Equation (89b) arises from the boundary conditions, and Eq. (89c) arises from the volume. The inverse Laplace transforms are obtained as described previously:

$$\phi=\frac{4\beta\epsilon\sigma(1-\delta)}{\pi}\int_0^1\frac{\cos(TX)\sqrt{1-X^2}\,\partial X}{\epsilon^2X^4[(1+\delta)^2-4\beta^2]+2\epsilon X^2[2(1-\beta^2)-\sigma(1-\delta^2)]+\sigma^2(1-\delta)^2} \tag{90a}$$
$$-\frac{2\sigma\mu(1-\delta)}{3\pi R_s\beta}\int_0^1\partial X\,X\sqrt{1-X^2}\sin(TX)\frac{A\epsilon^2X^4+B\epsilon X^2+C}{\{\epsilon^2X^4[(1+\delta)^2-4\beta^2]+2\epsilon X^2[2(1-\beta^2)-\sigma(1-\delta^2)]+\sigma^2(1-\delta)^2\}^2} \tag{90b}$$
$$-\frac{32\mu\sigma(1-\delta)}{3\pi R_s}\int_0^1\partial X\,X^2\sqrt{1-X^2}\,\Xi_C(T,X)\frac{\epsilon X^2(1+\delta)-\sigma(1-\delta)}{\{\epsilon^2X^4[(1+\delta)^2-4\beta^2]+2\epsilon X^2[2(1-\beta^2)-\sigma(1-\delta^2)]+\sigma^2(1-\delta)^2\}^2}\ , \tag{90c}$$

where

$$A=2[3(1+\delta)^3+8\beta^4(3+\delta)-4\beta^2(1-\delta)(5+2\delta)]\ , \tag{91a}$$
$$B=3(1+5\delta^2)-\beta^2(1-\delta)-9\beta^2\delta(1+\delta)-54\beta^2(1-\beta^2)+16\beta^4\delta-\sigma(1-\delta)[3(1+\delta)^2-4\beta^2(2-\delta-4\beta^2)] \tag{91b}$$
$$C=-2\sigma(1-\delta)\{8\beta^4+12(1-\beta^2)(3+\delta)-\sigma(1-\delta)[3(1+\delta)+4\beta^2]\}\ . \tag{91c}$$

In Zaidel's Eq. (2.8) (1967), the viscous perturbation has the form of Eq. (90b) but with different coefficients, and no term with the form of Eq. (90c).

VIII. SUMMARY OF APPROXIMATIONS

The approximations used in the previous sections, and in the Zaidel' (1967) development, are the following.

● *Initial conditions.* The initial conditions, Eq. (44), are clearly inexact, although they may suffice for the case $k_0\xi_0\ll 1$. They call for a well established smooth shock to be instantaneously perturbed without affecting the flow field behind the shock. In any real experiment the creation of a perturbed shock front will necessarily generate perturbations behind the front. This approximation is appropriate for the purposes of a stability analysis, but is inappropriate for the modeling of any real experiment.

● *Small-amplitude perturbations.* This approximation manifests itself in two ways. First, the boundary condition at the shock front applies at $x=\xi$ and not $x=0$. We have used the latter, and have therefore implicitly required ξ to be small. Second, we have assumed that long-wavelength perturbations greatly exceed shorter-wavelength perturbations. When $k_0\xi_0$ is large, these shorter-wavelength perturbation terms cannot be ignored. This assumption is not restrictive, since we can solve for other, shorter-wavelength, Fourier components of the solution.

● *Far-field boundary conditions.* To determine the function ξ as a function of time, an additional boundary condition is required. Zaidel' (1967) imagines a boundary infinitely far behind the shock front, and requires that all perturbations vanish at this point. In a real experiment there may be such a boundary at a finite distance behind the front, e.g., at the interface between the sample and the explosive, or the sample and the projectile in a gun experiment. The influence of the position of this boundary must be determined to assess the applicability of his approach. A test of this assumption can be made by comparing the results calculated above with the results for a corrugated shock generated by the motion of a corrugated piston against a fluid sample. Freeman (1955) and Zaidel' (1958) considered the latter problem and derived solutions for an inviscid fluid.

● *Negligible viscosity.* By treating viscosity as a perturbation to an inviscid solution, we restrict the form of the solution to linear combinations of the inviscid eigenvectors. It is not immediately apparent that these eigenvectors adequately describe the flow field in the viscous case. If the inviscid eigenvectors are demonstrably appropriate, then successively higher-order viscous perturbations could be used to get increasingly accurate estimates of the full viscous solution.

● *Bulk viscosity.* The bulk viscosity of water is greater than its shear viscosity at 1 bar (Liebermann, 1949). In Zaidel's (1967) analysis the bulk viscosity was neglected. According to the theory of absorption of sound (Landau and Lifshitz, 1959, pp. 298–302), the bulk viscosity and shear viscosity have approximately equal importance. If at high pressure the bulk and shear viscosities are similar in magnitude, this neglect could lead to factor-of-two errors, but not the several-order-of-magnitude discrepancies described previously.

● *Narrow shock width.* As discussed in Sec. II, the jump conditions employed in formulating the boundary conditions are exact only in the limit of a strictly discontinuous shock. The application of these conditions to viscous materials requires that the shock-front width be very small compared to the radius of curvature of the shock. This condition is readily satisfied in practice.

● *Linearizations.* Linearizing approximations include the adiabatic (isentropic) $\rho'-P'$ relationship and the Newtonian viscosity approximations. These approximations are adequate only when the strain rates and pressure perturbations are small, $k_0\xi \ll 1$.

Qualitatively, many aspects of the experimental results (Sakharov *et al.*, 1965; Mineev and Savinov, 1967) are predicted by the theory: the shock perturbation amplitude decays in an oscillatory manner, and the rate of this decay depends on the viscosity of the fluid. However, one important feature of our model is at odds with the experimental results. The experiments suggest that the function ϕ initially decays rapidly ($\dot{\phi}<0$ as $t\rightarrow 0$), but our theory predicts that $\dot{\phi}$ is initially positive (or slightly negative if $\kappa \gg \eta$). The reason for this discrepancy will be shown to be a consequence of the initial conditions in Secs. IX and X. Another important discrepancy is the effect of viscosity on the rate of damping. The experiments (Sakharov *et al.*, 1965) suggest that increasing viscosity (or, equivalently, decreasing the Reynolds number) causes the oscillations to damp more rapidly. In our theory, viscosity prolongs the oscillations. The reason for this discrepancy has not been determined.

Whether the viscosities calculated by the viscous perturbation method are reasonable depends in part on the validity of the viscous perturbation method for small but finite viscosity. This question is examined in Sec. XI.

IX. EFFECT OF FINITE PERTURBATION AMPLITUDE AND INITIAL CONDITIONS

Finite amplitude and initial conditions are intimately related, since as amplitude increases the initial perturbations must also increase. Finite amplitude and initial conditions are coupled in a second way as well. The solution Eq. (65) can be written

$$\vec{u}=\mathbf{S}^{-1}e^{\Lambda x}\left[e^{-\Lambda\xi}(\mathbf{S}\vec{u})_{x=\xi}+\int_{\xi}^{x}e^{-\Lambda\chi}(\mathbf{S}\vec{g})\partial\chi\right], \quad (92)$$

where we now specify the boundary conditions at the surface $x=\xi$, the true shock interface, rather than the approximation $x=0$. As before, we require that the perturbations vanish as $x\rightarrow\infty$, so the third component of the bracketed vector must vanish. When the initial conditions and viscosity are neglected, this reduces to the case in which the third component of $\mathbf{S}\vec{u}_{x=0}$ is zero, as before. When these terms are included, however, Eq. (92) differs from Eq. (65), giving a second finite-amplitude contribution.

The initial conditions are increasingly important as the product $k_0\xi_0$ becomes non-negligible (i.e., when the amplitude ξ_0 is comparable to or greater than the perturbation wavelength $2\pi/k_0$). An indication of the importance of these initial conditions can be gained by estimating an initial condition that is compatible with the boundary conditions. A simple family of solutions will be derived that is characterized by two adjustable parameters. The quantity α indicates how rapidly the initial perturbations decay away from the shock front, and the quantity S is the initial time decay of the shock front. A dimensional derivation of these quantities is presented in the next section.

Suppose that the initial flow parameters are of the form

$$v_x(t=0,x)=f_x(x)e^{ik_0y}=f_x^0e^{k_0(iy-\alpha x)}\,, \tag{93a}$$

$$iv_y(t=0,x)=f_y(x)e^{ik_0y}=f_y^0e^{k_0(iy-\alpha x)}\,, \tag{93b}$$

$$\frac{P(t=0,x)}{\rho v}=f_p(x)e^{ik_0y}=f_p^0e^{k_0(iy-\alpha x)}\,. \tag{93c}$$

From the inviscid boundary conditions, Eq. (42), it can be shown that

$$f_x^0=\frac{(\sigma-1)(1+\delta)}{\sigma(1-\delta)}\dot{\xi}_0\,, \tag{94a}$$

$$f_y^0=-k_0v(\sigma-1)\xi_0\,, \tag{94b}$$

$$f_p^0=\frac{-2(\sigma-1)}{\sigma(1-\delta)}\dot{\xi}_0\,. \tag{94c}$$

Defining the quantity

$$S=\frac{\dot{\xi}_0}{k_0v\xi_0}\,, \tag{95}$$

we see that the initial-condition contribution, Eq. (68b), becomes

$$k_0v\hat{\phi}_{\rm IC}=\frac{\beta^2(3+\delta)Sz+(1+\delta+2\beta^2)S\omega-\sigma(1-\delta)(1-\beta^2)}{[\beta^2z+\omega+\alpha(1-\beta^2)][(1+\delta)z^2+2\omega z+\sigma(1-\delta)]}\,. \tag{96}$$

which can be inverted via the transformation Eq. (81) into

$$\phi_{\rm IC}=\frac{2\beta\epsilon}{\pi}\int_0^1\frac{\partial X\sqrt{1-X^2}[(A_1\epsilon^2X^4+B_1\epsilon X^2+C_1)\cos TX-\mu X(D_1\epsilon X^2+E_1)\sin TX]}{\{\beta^4\epsilon^2X^4-2\beta^2\epsilon X^2[1-\alpha^2(1+\beta^2)]+[1-\alpha^2(1-\beta^2)]^2\}\{\epsilon^2X^4[(1+\delta)^2-4\beta^2]+2\epsilon X^2[2(1-\beta^2)-\sigma(1-\delta^2)]+\sigma^2(1-\delta)^2\}}\,, \tag{97}$$

where

$$A_1=-\beta^2\{S\alpha[(1+\delta)^2-4\beta^2]+\sigma(1-\delta)(1+\delta+2\beta^2)\}\,, \tag{98a}$$

$$\begin{aligned}B_1=&S\alpha\{(1+\delta)^2+4\beta^2(\delta+2\beta^2)+\beta^2\sigma(1-\delta)(1+\delta-2\beta^2)-\alpha^2(1-\beta^2)[(1+\delta)^2-4\beta^2]+\sigma(1-\delta)(1+\delta+2\beta^2)\}\\&-\alpha^2\sigma(1-\delta)(1-\beta^2)(1+\delta-2\beta^2)+\beta^2\sigma^2(1-\delta)^2\,,\end{aligned} \tag{98b}$$

$$C_1=-\sigma(1-\delta)[1-\alpha^2(1-\beta^2)][S\alpha(1+\delta+2\beta^2)+\sigma(1-\delta)]\,, \tag{98c}$$

$$D_1=2\beta^2\{S(1+\delta+2\beta^2)-S\beta^2\sigma(1-\delta)+S\alpha^2[(1+\delta)^2-4\beta^2]+\alpha\sigma(1-\delta)(2+\delta+\beta^2)\}\,, \tag{98d}$$

$$\begin{aligned}E_1=&-2\{S[(1+\delta+2\beta^2)-\alpha^2(1+\delta)-\alpha^2\beta^2(1-\delta-2\beta^2)-\beta^2\sigma(1-\delta)+\alpha^2\beta^2\sigma(1-\delta)(2+\delta+\beta^2)]\\&+\alpha\sigma(1-\delta)[(1-\beta^2)+\beta^2\sigma(1-\delta)-\alpha^2(1-\beta^2)^2]\}\,.\end{aligned} \tag{98e}$$

The transformation Eq. (81) is valid, i.e., the poles of Eq. (96) lie within the unit circle $|W|<1$, when Eq. (75) is satisfied and

$$|\beta\mu\alpha|<1\,. \tag{99}$$

If this condition is violated, i.e., if initial perturbations are attenuated more rapidly than $\exp[-(\beta\mu)^{-1}k_0x]$, an instability will develop.

Now Eq. (79) together with Eq. (97) gives an estimate of the shock-front perturbation in the inviscid limit subject to the initial conditions of Eq. (93). The finite amplitude of the shock front has not yet been considered. To account for the finite amplitude as a perturbation to the linear result we use Eq. (92). Requiring the solution to be finite as $x\to\infty$, we discover that ξ is given by the sum of Eq. (79) and the product $\exp(-\alpha k_0\xi)$ times Eq. (97), where the sum of Eqs. (79) and (97) is used in the exponential multiplier ξ':

$$\phi=\frac{4\beta\epsilon\sigma(1-\delta)}{\pi}\int_0^1\frac{\cos(Tx)\sqrt{1-x^2}dx}{\epsilon^2x^4[(1+\delta)^2-4\beta^2]+2\epsilon x^2[2(1-\beta^2)-\sigma(1-\delta^2)]+\sigma^2(1-\delta)^2}$$
$$+\frac{2\beta\epsilon\exp(-k_0\alpha\xi')}{\pi}$$
$$\times\int_0^1\frac{\partial X\sqrt{1-X^2}[(A_1\epsilon^2X^4+B_1\epsilon X^2+C_1)\cos TX-\mu X(D_1\epsilon X^2+E_1)\sin TX]}{\{\beta^4\epsilon^2X^4-2\beta^2\epsilon X^2[1-\alpha^2(1+\beta^2)]+[1-\alpha^2(1-\beta^2)]^2\}\{\epsilon^2X^4[(1+\delta)^2-4\beta^2]+2\epsilon X^2[2(1-\beta^2)-\sigma(1-\delta^2)]+\sigma^2(1-\delta)^2\}}\,. \tag{100}$$

This correction, and the effect of the approximate initial condition, is shown in Fig. 8.

A viscous perturbation to this solution can be obtained by using this result to estimate the shear stresses in the inviscid case. Using these estimates, one can derive a new viscous perturbation that takes account of the finite initial conditions. This viscous perturbation (Fig. 9) is readily determined by the methods described in Sec. VI. The resulting expressions are very lengthy, however, so they are not presented here. The initial slope of the vicious term $\dot{\phi}_{\rm visc}$ is

$$\lim_{t\to0}\dot{\phi}_{\rm visc}=\frac{2k_0v\sigma(\beta+\delta)}{R_s(1+\delta+2\beta)}$$
$$-\frac{\beta k_0v}{2R_b}\frac{S\alpha[(1+\delta)(1+6\delta+\delta^2+8\beta^2)+2\beta(1+3\beta)(3+\delta)]+\sigma(1-\delta)\{(1+6\delta+\delta^2)+2\beta[3(1+\delta)+2\beta]\}}{(1+\beta)(1-\delta)(1+\delta+2\beta)^2}\,. \tag{101}$$

When $S<0$, $\alpha>0$, and $0<\delta<1$, the initial slope will be positive. The influence of viscosity is again to initially amplify the shock-front perturbation relative to the inviscid case.

X. DIMENSIONAL ANALYSIS OF THE QUANTITIES α AND S

A simple dimensional argument can be made for the semiquantitative estimate of the parameters α and S that we hypothesize to characterize the initial shock perturbation structure. First recall the specific experimental geometry of Sakharov *et al.* (1965) (Figs. 1, 4, and 10). A section of sample material had a set of sinusoidal grooves cut in its upper surface. The planar surface of a wedge of identical sample material was then placed over these sinusoidal grooves. For fluid samples, thin metal or plastic containers were used to reproduce this geometry (Mineev and Zaidel', 1968). The containers themselves were assumed to have negligible impact on the perturbation development. A shock was initiated in the first, grooved sample. When the shock front reached the grooves, the shocked specimen began to release adiabati-

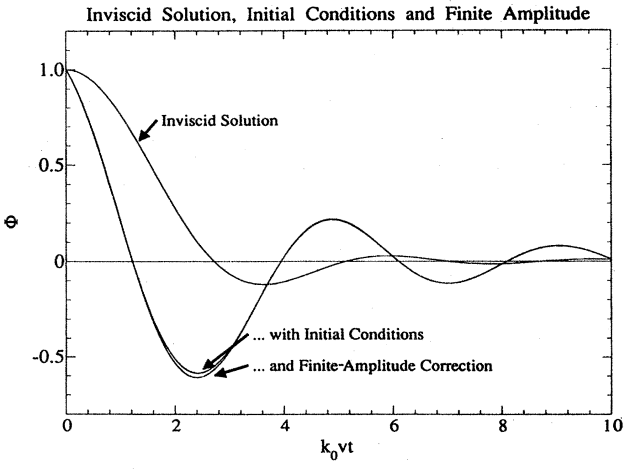

FIG. 8. Effect of approximate initial conditions [Eq. (97)] on the inviscid solution, with and without finite-amplitude correction [Eq. (100)], compared to inviscid solution without initial conditions [Eq. (79)]. Evaluated with parameters listed in Table I.

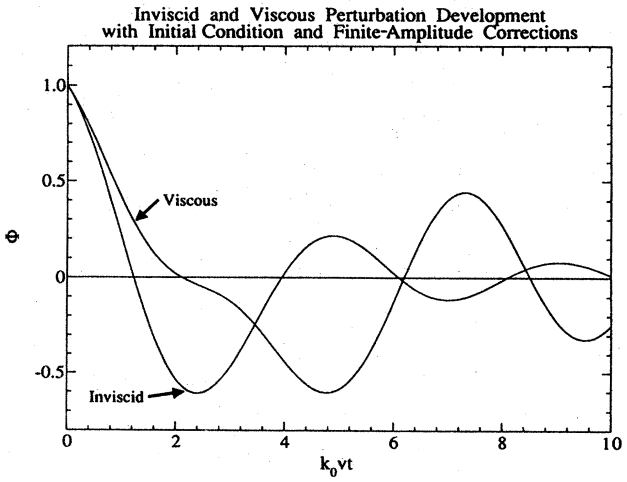

FIG. 9. Viscous perturbation calculation [Eq. (100) and viscous perturbation] compared to inviscid calculation [Eq. (100)], both with approximate initial conditions and finite-amplitude correction. Evaluated with parameters listed in Table I, $R_s=4.32$, and $\kappa=\eta$.

cally to ambient pressure. 180° out of phase with these releasing regions, the shock continued unperturbed to approach the upper sample wedge [Fig. 10(b)]. In the limit $k_0 \rightarrow 0$ the "normal" regions 180° out of phase with the releasing regions would be unaffected by this release process.

In the regions where release commences, the free surface will travel with velocity $\approx 2U_P$. In the "normal" region, the shock travels at a velocity U_S. In the weak shock limit, $\sigma < 2, U_S > 2U_P$ and the shock will reach the wedged sample before the released surface does. In this case, ξ_0 will be positive where the grooves were cut and negative where the sample material is continuous. ξ_0 will have the opposite phase if the stock is strong, $\sigma > 2$.

If the initial depth of the grooves is $2x_0$, i.e., the groove depth varies as $x_0[1-\cos(k_0 y)]$, then the initially released material will reach the wedge at a time

$$t_{\text{close}} = \frac{x_0}{U_P} , \tag{102}$$

the time necessary to close the sinusoidal void. In this same time, the shock wave will have traveled a distance

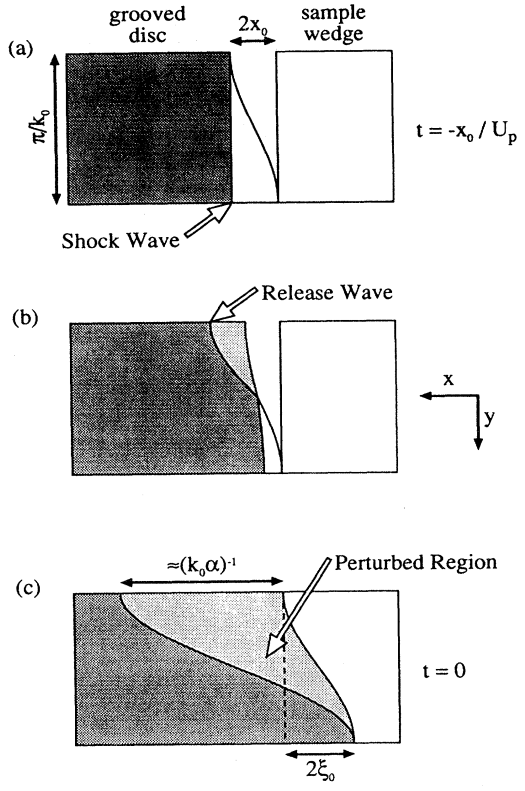

FIG. 10. Schematic of the development of perturbations in the shock front. When the shock first reaches the grooves in the sample disc (a), the sample will begin to release to ambient pressure. A release wave propagates backward into the shocked material as the shock wave progresses forward where the shock has not intersected the grooves (b). When the grooves are closed a sinusoidal perturbed shock front will have been generated (c), and a perturbed region will exist behind this shock front.

$$\frac{x_0 U_S}{U_P} , \tag{103}$$

or a distance

$$\frac{x_0(U_S - 2U_P)}{U_P} \tag{104}$$

into the wedge [Fig. 10(c)]. This is twice the initial amplitude of the shock-wave perturbation:

$$\xi_0 = \frac{x_0(U_S - 2U_P)}{2U_P} = \frac{x_0|2-\sigma|}{2(\sigma-1)} . \tag{105}$$

The initial amplitude ξ_0 is taken to be positive, so we use the absolute value $|2-\sigma|$. The sign of $(2-\sigma)$ determines the phase of ξ with respect to the grooves.

While the free surface is closing the void, a release wave is traveling in the opposite direction into the shocked material. This release wave travels at a velocity $(c - U_P)$ and will travel a distance

$$\frac{x_0(c - U_P)}{U_P} \tag{106}$$

away from the point of initial release, or a distance of

$$\frac{x_0(c + U_P)}{U_P} \tag{107}$$

relative to the first surface of the wedge at time t_{close}. The characteristic length scale of this initial disturbance is thus

$$\frac{1}{k_0\alpha} \approx \frac{x_0(c+U_P)}{U_P} = \frac{2[1+\beta(\sigma-1)]\xi_0}{\beta|2-\sigma|} , \tag{108}$$

or

$$\alpha \approx \frac{\beta|2-\sigma|}{2k_0\xi_0[1+\beta(\sigma-1)]} . \tag{109}$$

Sakharov *et al.* (1965) suggest that the length scale for the initial velocity perturbations will be on the order of ξ_0. According to this approximate analysis, the length scale will be approximately $1/(k_0\alpha) \approx 20 \times \xi_0$ for water at 15 GPa.

When the void first closes, a velocity perturbation will exist. Where a void had existed, material will have a velocity of $2U_P$, and where no void had existed material will have a velocity of U_P. In the coordinate frame of Zaidel' (1967), the initial velocity perturbation will be

$$2v_x' = -U_P = -v(\sigma-1) . \tag{110}$$

From Eqs. (94a) and (95) we then have

$$S = -\frac{\sigma(1-\delta)}{2(1+\delta)k_0\xi_0} . \tag{111}$$

The initial time derivative of ξ will therefore be negative for all stable shocks $\delta < 1$.

At the level of approximation considered here, both α and S are functions of the product $k_0\xi_0$. The impact of these "nonlinear" parameters may be experimentally as-

sessed, independently of viscous effects, by using different values of $k_0\xi_0$ and, independently, k_0 or ξ_0 (Sakharov *et al.*, 1965).

This approximate analysis gives approximate values of α and S that qualitatively reproduce the observed short-time behavior of the shock-front oscillations. It would be useful to derive more exact expressions for the initial shock and flow structure.

XI. COMPLETE VISCOUS SOLUTION

We noted in Sec. VIII that the perturbation approach may be overly restrictive in that only the inviscid eigenmodes of the system are considered. In going from the inviscid solution to a viscous solution, the governing differential equations change from first to second order, and the solution becomes correspondingly more complex. In the case of viscous flow, it is commonly observed that instabilities occur for certain critical Reynolds numbers. These so-called Tollmien-Schlichting instabilities (Schlichting, 1979) are most commonly associated with viscous boundary layers, since it is in this context that viscosity is most commonly encountered, but the phenomena may be relevant to the issue of shock stability as well.

The complete second-order differential equations that govern this problem may be solved to give a Laplace transform solution for the shock-front corrugation amplitude. This solution will be presented below. The solution $\hat{\phi}$ is algebraically complex, however, and is not as easy to interpret as was the inviscid solution. Because of this complexity, we resort to numerical solution methods. By way of some numerical examples, it will be shown that the complete second-order equations do indeed exhibit instabilities.

The second-order equations may be written as a set of five first-order equations by introducing the variables

$$q \equiv \frac{1}{k_0}\frac{\partial v_x}{\partial x} , \tag{112}$$

and

$$r \equiv \frac{1}{k_0}\frac{\partial v_y}{\partial x} . \tag{113}$$

Using these new variables, one can write the Laplace transformed equations of motion and continuity as

$$\frac{\partial}{\partial x}\begin{bmatrix} \hat{v}_x \\ i\hat{v}_y \\ \hat{P} \\ \rho v \\ \hat{q} \\ i\hat{r} \end{bmatrix} = k_0 \begin{bmatrix} 0 & 0 & 0 & 1 & 0 \\ 0 & 0 & 0 & 0 & 1 \\ 0 & -(1+\epsilon) & -z & -(1+\epsilon) & 0 \\ \frac{R_b}{R_s}(1+R_s z) & -R_b(1+\epsilon) & -R_b z & -R_b\epsilon & \frac{(R_b-R_s)}{R_s} \\ 0 & \frac{R_s}{R_b}(1+R_b z) & -R_s & \frac{(R_s-R_b)}{R_b} & R_s \end{bmatrix} \begin{bmatrix} \hat{v}_x \\ i\hat{v}_y \\ \hat{P} \\ \rho v \\ \hat{q} \\ i\hat{r} \end{bmatrix} + \begin{bmatrix} 0 \\ 0 \\ \frac{P}{\rho v^2} \\ R_b\left[\frac{P}{\rho v^2}-\frac{v_x}{v}\right] \\ -\frac{iR_s v_y}{v} \end{bmatrix}_{t=0} . \tag{114}$$

For simplicity, we shall neglect the initial conditions in the following development.

As before, we seek an eigenvalue expansion for this matrix equation. The characteristic equation obtained from this expansion factors into two parts. The first is dependent only upon the pure shear viscosity,

$$\lambda^2 - k_0 R_s \lambda - k_0^2(1+R_s z) = 0 , \tag{115}$$

giving eigenvalues

$$\lambda_1 = \frac{k_0}{2}[R_s - \sqrt{R_s^2+4(1+R_s z)}] \tag{116a}$$

and

$$\lambda_2 = \frac{k_0}{2}[R_s + \sqrt{R_s^2+4(1+R_s z)}] . \tag{116b}$$

The first eigenvalue, λ_1, leads to decay of the perturbations for any real positive z, whereas the second solution will lead to exponential growth. In the inviscid limit, this part of the characteristic equation gave the single root λ_1 of Eq. (57).

The second factor of the characteristic equation is dependent solely on the viscosity accompanying compression without shear:

$$\lambda^3 + k_0\lambda^2(R_b\epsilon+z) - k_0^2\lambda(1+2R_b z) - k_0^3[R_b(1+\epsilon+z^2)+z] = 0 . \tag{117}$$

The roots of this cubic equation are algebraically complex:

$$\frac{\lambda_3}{k_0} = -2\sqrt{a}\cos\left[\frac{\theta}{3}\right] - \frac{R_b\epsilon+z}{3} , \tag{118a}$$

$$\frac{\lambda_4}{k_0} = -2\sqrt{a}\cos\left[\frac{\theta+2\pi}{3}\right] - \frac{R_b\epsilon+z}{3} , \tag{118b}$$

$$\frac{\lambda_5}{k_0} = -2\sqrt{a}\cos\left[\frac{\theta+4\pi}{3}\right] - \frac{R_b\epsilon+z}{3} , \tag{118c}$$

where

$$a \equiv \frac{(R_b\epsilon+z)^2+3(1+2R_bz)}{9} , \tag{119a}$$

$$b \equiv \frac{2(R_b\epsilon+z)^3+9(R_b\epsilon+z)(1+2R_bz)-27[R_b(1+\epsilon+z^2)+z]}{54} \tag{119b}$$

and

$$\theta \equiv \arccos\frac{b}{\sqrt{a^3}} . \tag{119c}$$

The root λ_4 is positive for real positive values of z and will therefore lead to instability. Both λ_3 and λ_5 are negative for real positive z and might therefore be acceptable solutions. For complex z, however, the phase of λ_3 indicates that it corresponds to waves incident upon the shock, whereas λ_5 corresponds to waves emitted by the shock. λ_3 might therefore be excluded on the grounds that it is unphysical. In the inviscid limit, the two eigenvalues associated with these acoustic modes were λ_2 and λ_3 of Eq. (57).

The complete boundary conditions at the shock front may be written as

$$u_{x=0} \equiv \begin{bmatrix} \hat{v}_x \\ i\hat{v}_y \\ \hat{P}/(\rho v) \\ \hat{q} \\ i\hat{r} \end{bmatrix}_{x=0} = \begin{bmatrix} \dfrac{-\xi_0(\sigma-1)(1+\delta)R_bR_s^2+\hat{\xi}k_0v(\sigma-1)R_s[zR_bR_s(1+\delta)-\sigma\delta(2R_b-R_s)]-R_s^2\sigma\delta\hat{q}+\sigma\delta(2R_b-R_s)i\hat{r}}{\sigma[R_bR_s^2(1-\delta)+\delta(2R_b-R_s)]} \\ \dfrac{\xi_0(\sigma-1)(1+\delta)R_bR_s-\hat{\xi}k_0v(\sigma-1)R_bR_s[z(1+\delta)+R_s\sigma(1-\delta)]+R_s\sigma\delta\hat{q}+\sigma(1-\delta)R_bR_si\hat{r}}{\sigma[R_bR_s^2(1-\delta)+\delta(2R_b-R_s)]} \\ \dfrac{-\xi_0(\sigma-1)[2R_b(1-R_s^2)-R_s]+\hat{\xi}k_0v(\sigma-1)[z(2R_b(1-R_s^2)-R_s)+\sigma R_s(2R_b-R_s)]+\sigma R_s^2\hat{q}-\sigma(2R_b-R_s)i\hat{r}}{\sigma[R_bR_s^2(1-\delta)+\delta(2R_b-R_s)]} \\ \hat{q} \\ i\hat{r} \end{bmatrix}_{x=0} \tag{120}$$

Recall that the boundary conditions in the inviscid case are underspecified, that is, $\hat{v}_{x,x=0}, \hat{v}_{y,x=0}$, and $\hat{P}_{x=0}$ are not uniquely defined, but are functions of $\hat{\xi}$. By omitting one eigenmode from the solution, we acquired an addition constraint, and it became possible to determine $\hat{\xi}$. In the present case, our boundary conditions are underspecified to a greater extent: we have the three boundary values $\hat{\xi}, \hat{q}_{x=0}$, and $\hat{r}_{x=0}$ that are undetermined. By omitting three of the five eigenmodes from the solution, we satisfy the necessary constraints. Applying the methodology described previously, we may determine the behavior of the shock front by simultaneously solving

$${}^l\Psi_2 \cdot u_{x=0} = 0 , \tag{121a}$$

$${}^l\Psi_3 \cdot u_{x=0} = 0 , \tag{121b}$$

$${}^l\Psi_4 \cdot u_{x=0} = 0 \tag{121c}$$

for the three unknowns $\hat{q}_{x=0}$, $\hat{r}_{x=0}$, and $\hat{\xi}$, where ${}^l\Psi_n$ is the left eigenvector corresponding to λ_n.

An alternative formulation of the solution is to expand the velocity and pressure perturbations in terms of the right eigenvectors,

$$u = C_1{}^r\Psi_1 + C_5{}^r\Psi_5 , \tag{122}$$

where ${}^r\Psi_n$ is the right eigenvector corresponding to eigenvalue λ_n. This alternative approach, formally identical to the earlier method, is somewhat less awkward in this case.

We begin by taking appropriate linear combinations of the boundary conditions to obtain

$$k_0v\hat{\xi}(\sigma-1)z = (\sigma-1)\xi_0+\sigma\left[\hat{v}_x+\delta\frac{\hat{P}}{\rho v}\right] , \tag{123a}$$

$$R_s\hat{q} = 2R_bR_s\hat{v}_x+(2R_b-R_s)i\hat{v}_y+R_bR_s(1+\delta)\frac{\hat{P}}{\rho v} , \tag{123b}$$

and

$$iz\hat{r} = R_s(\sigma-1)\xi_0+(R_s\sigma+z)\hat{v}_x+R_szi\hat{v}_y+R_s\sigma\delta\frac{\hat{P}}{\rho v} \tag{123c}$$

at $x=0$. The last two conditions, in conjunction with Eq. (122), may be used to determine the coefficients C_1 and C_5. Defining

$$\vec{\Phi}_1 = \begin{bmatrix} 2R_bR_s \\ 2R_b-R_s \\ R_bR_s(1+\delta) \\ -R_s \\ 0 \end{bmatrix} \quad \text{and} \quad \vec{\Phi}_2 = \begin{bmatrix} R_s\sigma+z \\ R_sz \\ R_s\sigma\delta \\ 0 \\ -z \end{bmatrix} , \tag{124}$$

we write

$$M \equiv \begin{bmatrix} {}^r\Psi_1\cdot\Phi_1 & {}^r\Psi_5\cdot\Phi_1 \\ {}^r\Psi_1\cdot\Phi_2 & {}^r\Psi_5\cdot\Phi_2 \end{bmatrix} , \tag{125a}$$

$$M \begin{bmatrix} C_1 \\ C_5 \end{bmatrix} = \begin{bmatrix} 0 \\ -R_s(\sigma-1)\xi_0 \end{bmatrix} \tag{125b}$$

to determine the coefficients C_1 and C_5. These coefficients, together with Eq. (122), serve to determine $\hat{v}_x$ and $\hat{P}/(\rho v)$, which may be used to solve for $\hat{\xi}$ with Eq. (123a).

The right eigenvectors are

$${}^r\Psi_1 = \begin{bmatrix} 1 \\ -\lambda_1' \\ 0 \\ \lambda_1' \\ -\lambda_1'^2 \end{bmatrix} \quad \text{and} \quad {}^r\Psi_5 = \begin{bmatrix} -\lambda_5'(\lambda_5'+z) \\ (\lambda_5'+z) \\ -(1+\epsilon)(1-\lambda_5'^2) \\ -\lambda_5'^2(\lambda_5'+z) \\ \lambda_5'(\lambda_5'+z) \end{bmatrix} , \tag{126}$$

leading to the solution

$$k_0 v\hat{\phi} = -\frac{R_b\{(\lambda_5'+z)[4(1+R_sz-\lambda_5'\lambda_1')+2R_s(\lambda_1'-R_s+z)+R_s(R_sz-2)(z-\lambda_5')]-R_s\delta(1+\epsilon)(1-\lambda_5'^2)(R_sz+2)\}}{\det(M)} , \tag{127}$$

where

$$\det(M) = -R_b\{R_s\delta(1+\epsilon)(1-\lambda_5'^2)[R_s(\sigma-z^2)-2(\lambda_1'\sigma+z)] + (\lambda_5'+z)[2(1+R_sz-\lambda_5'\lambda_1')(R_s\sigma+2z)+2R_sz(\lambda_1'-R_s+z)+R_s(z-\lambda_5')(R_sz^2-2z-R_s\sigma)]\} , \tag{128}$$

and λ_i' is λ_i/k_0.

In this inviscid limit, $R_s\to\infty$ and $R_b\to\infty$, the eigenvalues correspond to those derived in the previous section [Eq. (57)]. The solution $\hat{\phi}$ is also identical to the inviscid solution, Eq. (68a), obtained in the previous sections. The D'yakov-Kontorovich stability criteria are therefore applicable in this case.

If we seek approximate solutions for λ_1 and λ_5 in the form of power-series expansions, e.g.,

$$\lambda_1 \approx -k_0 z - \frac{k_0(1-z^2)}{R_s} + O(R_s^{-2}) \tag{129a}$$

and

$$\lambda_5 \approx \frac{k_0(\beta^2 z-\omega)}{(1-\beta^2)} + \frac{k_0\beta^4(z-\omega)^3}{2R_b(1-\beta^2)^3\omega} + O(R_b^{-2}) , \tag{129b}$$

and write a Taylor-series expansion for $\hat{\phi}$,

$$\hat{\phi} \approx \lim_{R_s\to\infty,R_b\to\infty}\hat{\phi} + R_s^{-1}\lim_{R_s\to\infty,R_b\to\infty}\left[\frac{\partial\hat{\phi}}{\partial R_s^{-1}}\right] + R_b^{-1}\lim_{R_s\to\infty,R_b\to\infty}\left[\frac{\partial\hat{\phi}}{\partial R_b^{-1}}\right] , \tag{130}$$

then we arrive at the same solution, Eq. (82), obtained by the perturbation method of Zaidel' (1967), valid in the limit of negligible viscosity.

The limit of infinite viscosity may also be obtained from Eq. (127). In the limit $R_s\to 0$, the characteristic equation (115) gives the two solutions

$$\lambda = \pm k_0 , \tag{131}$$

where the negative solution is the stable one. When $R_b\to 0$, the acoustic characteristic equation (117) gives the three solutions

$$\lambda = -k_0 z, \pm k_0 . \tag{132}$$

The two negative roots are unconditionally stable; however, only the root $\lambda=-k_0z$ gives an eigenvector that is linearly independent of the entropy waves.

The shock-front perturbation in this limit is

$$\lim_{R_s\to 0,R_b\to 0} k_0 v\hat{\phi} = \frac{1}{z} . \tag{133}$$

Thus the shock-front perturbation amplitude is a unit step function,

$$\lim_{R_s\to 0,R_b\to 0}\phi = 1 \quad \text{for } t>0 . \tag{134}$$

The amplitude will neither grow nor diminish with time and is therefore unconditionally stable. This limiting behavior is very different from that indicated by the linearized perturbation method and indicates the limitations of that method for large but finite viscosity.

To study the solution for finite viscosity requires that the inverse Laplace transform of Eq. (127) be found. Because of the complexity of this equation, we employ the Legendre polynomial quadrature method of Bellman *et al.* (1966) to numerically invert Eq. (127). This inversion is shown in Fig. 11 for several values of R_s, with R_b determined by specifying $\kappa=\eta$. When R_s is large, i.e., 128 or larger, the solution approaches the inviscid solution (without initial conditions or finite-amplitude corrections). When R_s is 4, the solution is approximately critically damped: the oscillations of ϕ about zero are greatly

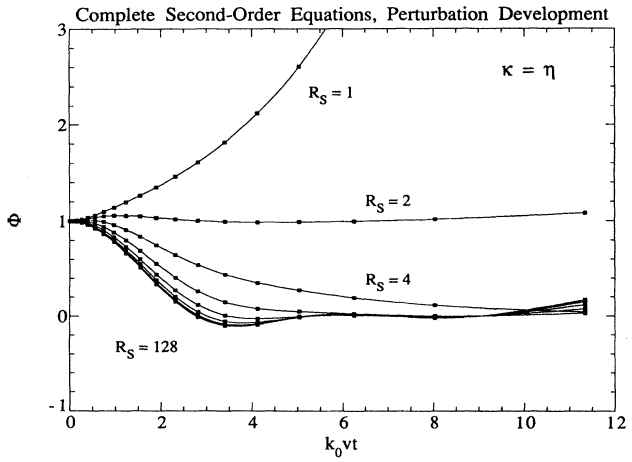

FIG. 11. Numerical inversion of second-order equation [Eq. (127)] for $\kappa=\eta$ and $R_s=1,2,4,8,16,32,64$, and 128, with parameters listed in Table I. The squares represent the points calculated by the twentieth-order shifted Lagrange polynomial quadrature method (Bellman *et al.*, 1966), and the curves are fit to the points with cubic splines. Shear Reynolds numbers smaller than 4 appear to give unstable solutions. Large-shear-Reynolds-number solutions approach the inviscid solution given by Eq. (79), Fig. 5.

reduced. Smaller shear Reynolds numbers lead to qualitatively different behavior. As R_s approaches zero (not shown), the amplitude tends to remain constant at $\phi=1$ but ultimately to become unstable as for the case $R_s=1$ shown in Fig. 11. All of the numerical experiments conducted so far with $0<R_s<4$ ultimately exhibit instabilities.

Viscosity can usually be considered as a stabilizing factor, as in the case of flow through a pipe. When the Reynolds number is larger than some critical value, or, equivalently, the viscosity is too small, turbulence develops. Small Reynolds numbers or large viscosities give laminar flow. The opposite behavior is exhibited in this corrugated shock problem. One interpretation of this behavior comes from the analysis of Freeman (1955) of a related problem, that of a shock driven by a corrugated piston in an inviscid fluid. He identified the mechanism of shock perturbation decay as the interference of pressure (sound) waves at the shock front. If these pressure waves were strongly attenuated, as in a highly viscous fluid, then the damping mechanism would be ineffective.

These instabilities are kinetic in origin and as such are fundamentally different from those that arise from violation of the Kontorovich-D'yakov criteria. The latter, which are thermodynamic in origin, lead to shock-splitting. We infer, by analogy to Tollmien-Schlichting instability theory, that these low-Reynolds-number instabilities lead to turbulence at the shock front. Since there is a wavelength for any viscous material such that R_s will be less than 4, these calculations predict that turbulence may occur commonly in shock experiments. Whether such turbulence is detectable would depend on the wavelength of the perturbation and the magnitude of the viscosity, in addition to the thermodynamic parameters that characterize the system. The possible existence of such turbulence at the shock front suggests the possibility of more vigorous mixing than that occurring in the low-viscosity case (Fig. 6).

These mechanisms might explain the rapid dynamic mixing that is observed in shock-induced chemical reactions (see, for example, Boslough, 1989, 1990). Also, on a much larger scale, this turbulent mixing may play a role in the homogenization of impact-generated melts. Such melts can be compositionally homogeneous over tens of kilometers, although the target may be lithologically heterogeneous (Grieve and Floran, 1978).

XII. REVIEW OF EXPERIMENTS ON WATER

As an example, we shall examine the experimental results for water shocked to 15 GPa, the maximum shock pressure achieved in the viscosity measurement experiments of Mineev and Zaidel' (1968). The Hugoniot is given by $\rho_0=0.998$ g/cc, $c_0=2.393$ km/s, and $s=1.333$ ($U_S=c_0+sU_P$) (Mitchell and Nellis, 1982), valid in the range $1.5<U_P<7.1$ km/s. At a peak shock pressure of 15 GPa, the linear U_S-U_P relation gives $U_S=5.383$ km/s and $U_P=2.243$ km/s. v is then 3.140 km/s, v_0 is 5.383 km/s, and σ is 1.714.

The Hugoniot bulk modulus can be determined from the U_S-U_P shock equation of state:

$$K_H\equiv -V\frac{\partial P}{\partial V}\bigg|_{\text{Hugoniot}}=\frac{U_S}{V_0}(U_S-U_P)\left[\frac{U_S+U_PU_S'}{U_S-U_PU_S'}\right], \tag{135}$$

where U_s' is $\partial U_S/\partial U_P$, or s for a linear (i.e., $U_S=c_0+sU_P$) material. This relationship allows δ, Eq. (33), to be calculated from

$$\delta=\frac{U_S-U_PU_S'}{U_S+U_PU_S'}=\frac{\sigma-s(\sigma-1)}{\sigma+s(\sigma-1)}, \tag{136}$$

from which we calculate $\delta=0.287$ at 15 GPa.

Bakanova *et al.* (1976) measured the sound speed of shock-compressed water, and a value of 5.8 km/s is given by their results at 15 GPa. Using this experimentally constrained sound speed, one finds β to be 0.541.

The initial amplitude of the perturbations is reported to be in the range $k_0\xi_0=0.19$ to 1.13. From Eq. (109) we then estimate α to be in the range 0.34 to 0.06 and, from Eq. (111), S to be in the range -2.50 to -0.42.

Mineev and Zaidel' (1968) calculate a viscosity of 2.2×10^4 poise with perturbation wavelengths of 1 and 2 cm. The shear Reynolds number (R_s) that characterizes this problem, Eq. (83), is then 4.23 ($2\pi/k_0=1$ cm) or 8.46 ($2\pi/k_0=2$ cm). Note that the viscous perturbation method is valid in the limit $R_s,R_b\to\infty$.

The conditions (75) and (99) for the transformation contours are satisfied.

Viscosities were obtained from the Sakharov *et al.* (1965) type of experiments by conducting two experiments with different Reynolds numbers and measuring the difference in normalized time of the first zero crossing of ϕ. This doubling allows viscous effects (dependent on k_0, but independent of $k_0\xi_0$) to be separated from finite-amplitude effects (dependent on $k_0\xi_0$, but independent of k_0) and other complicating factors (i.e., yield strength). Doubling the Reynolds number for water at 15 GPa shifted the zero crossing by $k_0 v\Delta t = 0.59$ [Mineev and Zaidel' (1968) report $k_0 v_0 \Delta t/2\pi = 0.16$]. Figure 12 shows the calculated shift in zero crossing times for a doubling of the Reynolds number as a function of R_s^{-1}. When initial conditions are neglected, the perturbation theory predicts $R_s^{-1} = 0.078$ [Fig. 12(a)], assuming $\kappa = \eta$, from which η is found to be 6700 poise ($k_0 = 2\pi$). With these same assumptions, the second-order analysis predicts $\eta = 5800$ poise [Fig. 12(d)]. The perturbation method gives essentially the same result, within an order of magnitude, as the more exact second-order equations. The effect of the approximate initial conditions is to predict somewhat larger viscosities: 19 000 poise without the finite-amplitude correction [Fig. 12(b)] and 20 000 poise with the finite-amplitude correction [Fig. 12(c)]. These results are summarized in Table II. For all model calculations, increasing κ/η predicts a slight decrease in η.

These large calculated values of viscosity appear to be robust in the sense that different levels of approximation give similar values to within an order of magnitude.

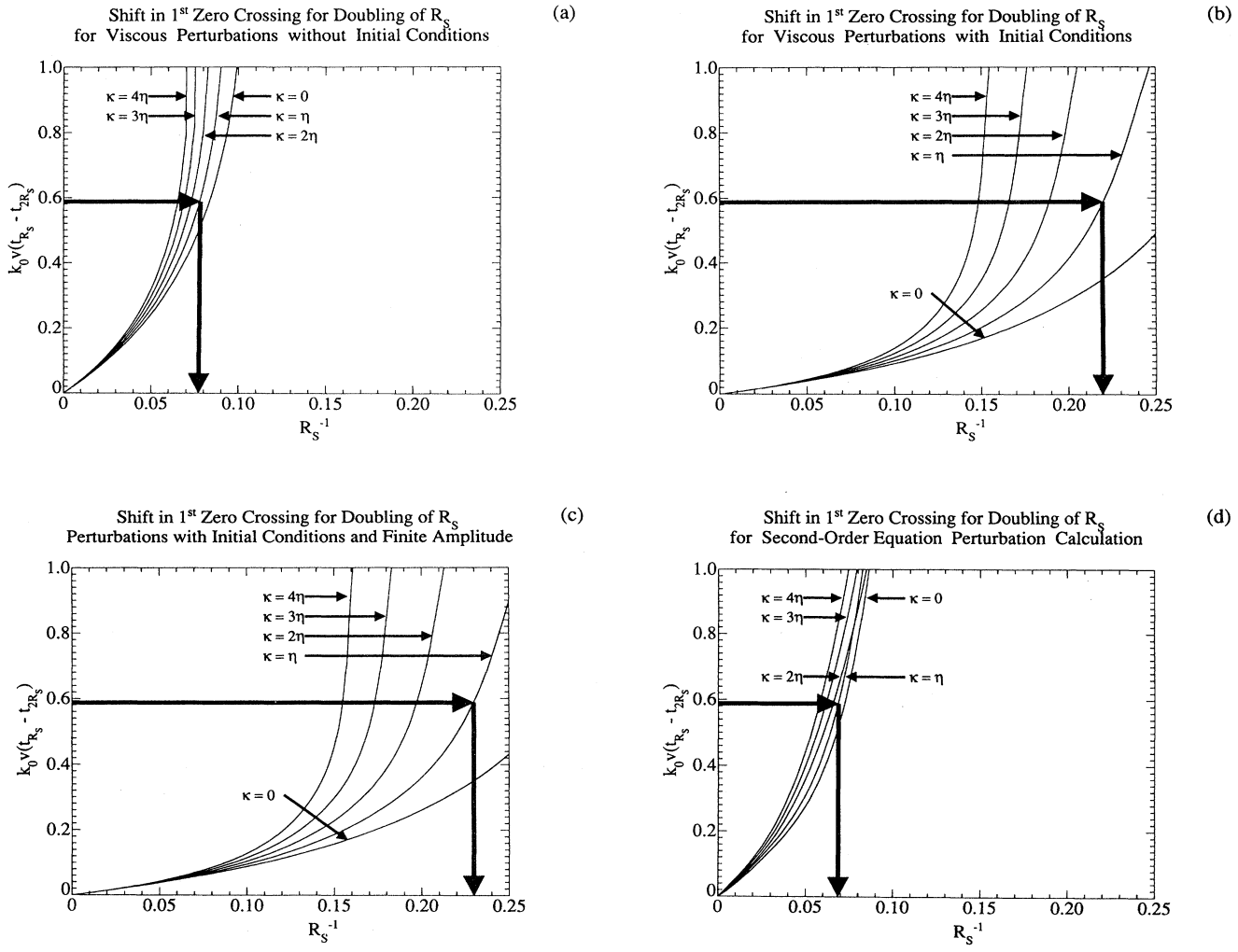

FIG. 12. Shift in time of first zero crossing for a doubling of the shear Reynolds number as a function of $1/R_s$ for $\kappa = 0$, η, 2η, 3η, and 4η, for (a) viscous perturbation method without initial conditions, (b) perturbation method with approximate initial conditions, (c) perturbation method with approximate initial conditions and finite-amplitude correction, and (d) second-order equation without initial conditions. Curves are calculated for water at 15 GPa, with $k_0\xi_0 = 1$, $k_0 = 2\pi\text{cm}^{-1}$, and parameters listed in Table I. Large arrows illustrate the calculation of shear Reynolds number from a set of experiments. Doubling the Reynolds number by doubling the perturbation wavelength shifts the first zero crossing of ϕ in dimensionless time ($k_0 vt$). For water at 15 GPa, this shift is 0.59. Assuming $\kappa = \eta$, the shear Reynolds number is 12.8 (a), corresponding to a shear viscosity of 6700 poise (with parameters of Table III).

TABLE II. Calculated shear viscosities for water at 15 GPa.

Method	Shear viscosity (poise)
Mineev and Zaidel' (1968) with viscous perturbation method of Zaidel' (1967)	22 000
Viscous perturbation [Eq. (86), Fig. 12(a)]	6700[a]
Viscous perturbation with approximate initial conditions [Eq. (97) and perturbation of Eq. (100), Fig. 12(b)]	19 000[a]
Viscous perturbation with initial conditions and finite-amplitude correction [Eq. (100) and perturbation, Fig. 12(c)]	20 000[a]
Second-order solution without initial conditions [Eq. (127), Fig. 12(d)]	5800[a]

[a] $\kappa=\eta$ is assumed.

While the addition of an initial-condition model reconciles the shape of $\phi(T)$ with the experimental data [assumed to be qualitatively similar to the published results for aluminum (Sakharov *et al.*, 1965; Mineev and Savinov, 1967)], its impact on the resulting viscosity calculation is unimportant in this case.

The good agreement between our calculations and the results of Mineev and Zaidel' (1968) demonstrates that the differences between our formulae and Zaidel's (1967) are minor, yet the calculated viscosities are substantially higher than other measurements and calculations (Fig. 3). One possible explanation for this many-order-of-magnitude discrepancy is that some other dissipative mechanism may act on the shock front (Hamann and Linton, 1969). One such mechanism is thermal conduction. Zaidel' (1967) noted that the combined equations of motion and continuity that govern this problem also, together with an equation of energy, describe the classical dissipation of sound (Landau and Lifshitz, 1959, pp. 298–302) by viscosity and thermal conductivity. This analysis predicts that the absorption coefficient for sound is proportional to

$$\frac{4}{3}\nu+\frac{\kappa}{\rho}+\alpha_P\gamma\chi T\ , \tag{137}$$

where κ is the bulk viscosity, α_P is the thermal expansivity at constant pressure, γ is the thermodynamic Grüneisen parameter, χ is thermal diffusivity, and T is the shock temperature. Indeed, we have found the terms $\frac{4}{3}\nu+(\kappa/\rho)$ to be the relevant viscosity for that part of the induced fluid motion associated with sound waves (e.g., Eq. 82). We might suppose that this association of parameters, including thermal conductivity, might effect the damping of the perturbed shock front. In this case, for the thermal diffusivity to be important $\alpha_P\gamma\chi T$ would need to have magnitude $O(\nu)$ to have a significant impact on the viscosity measurement. At low pressure, acoustic absorption in water by thermal conductivity is about 10^3 times less than by viscosity (Bhatia, 1967), thus it is doubtful that thermal conductivity is responsible for the large effective viscosities.

Mineev and Zaidel' (1968) attribute the large viscosity measured under these conditions to the high frequency of the perturbations relative to the relaxation time of the sample, i.e., they propose $\tau\geq 1/\dot{\epsilon}$ where $\dot{\epsilon}$ is the strain rate. They estimate this strain rate to be

$$\dot{\epsilon}\approx k_0^2 v_0 \xi_0\ , \tag{138}$$

which they calculate to be on the order of 0.1 MHz, corresponding to a characteristic time of 10 μs. Another measure of the characteristic frequency of perturbations comes from the acoustic frequency,

$$\Omega=c\sqrt{k_0^2+\mathrm{Im}[\lambda_{\mathrm{acoustic}}]^2}\ , \tag{139}$$

evaluated at the poles of Eq. (68). These poles are readily determined from the denominator of Eq. (74) with the transformation Eq. (72) and give a characteristic acoustic frequency of 4.8 MHz and time scale 0.22 μs with the parameters in Table I. If water has an anelastic absorption mode near 4.8 MHz, then sound waves will be attenuated as if by viscosity, and the effective viscosity calculated by the method described above will therefore greatly overestimate the bulk and shear viscosities.

Harris and Presles (1981) suggested that the Sakharov *et al.* (1965) experiments appear to measure shock-front-related viscosity. Indeed, our analysis does suggest that the viscosity at the shock boundary does have a greater influence over the damping than does the viscosity in the bulk of the shocked fluid. Figure 7(a) shows the shock-front contributions [Eqs. (86b) and (86c)] and volume contributions [Eqs. (86d), (86e), and (86f)] to the viscous perturbation (initial conditions neglected). Clearly the magnitude of the boundary condition term is comparable to that of the bulk, and more importantly it is of opposite sign. This calculation suggests that a viscosity at the surface of magnitude 10^4 poise and a viscosity in the volume of magnitude 10^{-2} poise would explain the experimental results while allowing for the possibility that the shear viscosity could be as small as 10^{-2} poise. To the extent that the material properties near the shock front may differ from those farther away, the shock-front perturbation method is subject to the same objections we raised concerning the shock profile methods.

If the material properties of the sample near the shock front were different from those in the bulk, the surface viscosity might be much greater than the viscosity in the

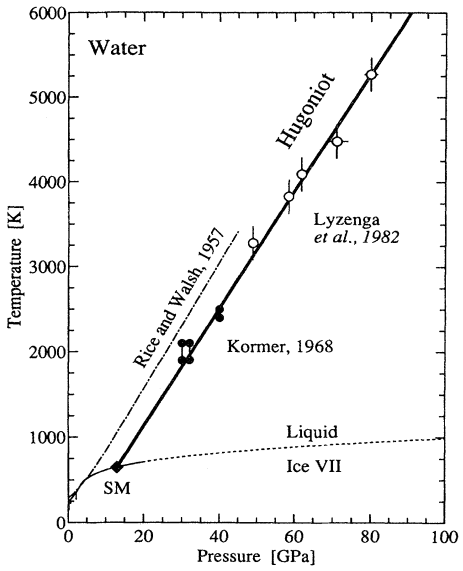

FIG. 13. Phase diagram for water (Pistorius *et al.*, 1963; Liu and Bassett, 1986), and calculated Hugoniot temperature for water (Rice and Walsh, 1957). More recent calculations by Schroeder and McMaster (1972) (SM) indicate that ice VII melts on the 20 °C initial-temperature Hugoniot at 13 GPa. The −10 °C initial-temperature Hugoniot is calculated to melt at 23.4 GPa. The shock-temperature measurements of Kormer (1968) and Lyzenga *et al.* (1982) support the high melting temperature calculation of Schroeder and McMaster.

volume. Rice and Walsh (1957) recognized that the Hugoniot for water passes through (or very near) the field of ice VII stability (Fig. 13). More recent experiments by Al'tshuler *et al.* (1958) and analyses by Schroeder and McMaster (1973) suggests that water does actually freeze to ice VII on the Hugoniot and melts at higher shock pressure. If this is true, then crystalline or partially crystalline water in (or near) the shock front could easily have a higher viscosity than the crystal-free liquid away from the front. This effect might influence the shock viscosity at higher pressure than the point at which ice VII melts on the water Hugoniot: ice VII formed on the Rayleigh path through the shock front might exist even if the final shock state were outside the field of ice VII stability. The existence of a phase transformation on the Rayleigh path would also have an adverse effect on the estimation of viscosity from the shock-front profile.

Mineev and Savinov (1976) discussed the shock viscosity of water in relation to its phase diagram. They noted that the measured viscosity of water decreases by about a factor of 5 in the range 12–25 GPa, but remains on the order of 10^4 poise. This large viscosity was attributed to the existence of ice VII. They suggested that melting did not occur abruptly on the Hugoniot, but occurred gradually with increasing pressure. While it is possible that water remains in the two-phase region over an extended pressure interval, this interpretation is inconsistent with the experimental results of Al'tshuler *et al.* (1958) and the calculations of Schroeder and McMaster (1973) that indicate complete melting by 13 GPa. Our suggestion that the material properties near the shock front may dominate reconciles Mineev and Savinov's (1976) interpretation with the phase relations.

If water were partially crystallized near 15 GPa on the Hugoniot, then indirect viscosity measurements, e.g., the electrical conductivity experiments (Hamann and Linton, 1969), might well predict a substantially lower viscosity than the oscillatory damping method. Even if ice VII existed at equilibrium with water behind the shock front, the existence of a fully interconnected melt network might give essentially the same conductivity measurement as a completely liquid system. Partially crystalline water behind the shock front would have an adverse effect on the viscous drag experiments (Al'tshuler *et al.*, 1977, 1986; Kim, 1984) as well, although these experiments should be insensitive to the material properties near the shock front itself.

XIII. CONCLUSIONS

We have expanded upon the analysis of Zaidel' (1967) for the damping of perturbations on a shock front. We have also clarified the assumptions implicit in the analysis and explored the ramifications of these assumptions on the application of the method to analyzing experiments. We considered in detail (1) the effect of initial conditions, (2) finite shock amplitude, (3) bulk viscosity, and (4) the validity of the viscous perturbation approach.

The controversial experiments on shocked water (Mineev and Zaidel', 1968) were reviewed. To the extent that we can analyze these experiments from the published descriptions, we conclude that the dissipative forces in the system are compatible with the viscosities calculated from the Zaidel' (1967) formulae. That this calculated viscosity may be apparent rather than real is suggested by the sensitivity of the calculation to the material properties in and near the shock front and the prediction that water may be at least partially crystalline (ice VII) on the Rayleigh path. This explanation could reconcile the Mineev and Zaidel' (1968) experiments with the viscosity estimates obtained from electrical conductivity measurements of dilute salt solutions.

If water has an anelastic absorption mode near 4.8 MHz, this too would lead to a gross overestimation of the viscosity. However, low-pressure studies do not indicate the existence of such modes in water (Herzfeld and Litovitz, 1959). The importance of anelasticity might be tested experimentally by conducting these experiments with longer-wavelength perturbations that give lower compressional wave frequencies.

It is important to note that the complete experimental measurements for $\phi(T)$ have not been published for any fluid, including water. Only the results for aluminum have been shown by Sakharov *et al.* (1965) and Mineev and Savinov (1967). In the case of aluminum, decreasing the Reynolds number shifts the first zero of ϕ to shorter

times. This is qualitatively opposite to our calculations for water. Since only the magnitude, and not the sign, of this phase shift for water has been reported, it remains to be shown whether or not the analytic description of the experiment even qualitatively models the data. Until such a comparison can be made to demonstrate good agreement between the theory and experiment, these calculated viscosities must be regarded as provisional.

The possibility that the experimental conditions were significantly different from the idealization of the analytical model is suggested by this serious discrepancy between theory and experiment (Godunov *et al.*, 1971). However, Godunov *et al.* (1976) add the caveat that the objection of Godunov *et al.* (1971) to the Sakharov *et al.* (1965) type of experiments applies only to those experiments for which $k_0\xi_0$ was of order unity. Since substantially similar viscosities are found for water with $k_0\xi_0$ ranging from 0.19 to 1.13, the importance of this initial-condition discrepancy may be questionable. Additional experimentation is required to characterize the initiation of the shock perturbations and assess the suitability of the analytic model.

The oscillatory damping experiments were originally suggested as a method for determining shear viscosity at high pressure. We have shown that bulk viscosity influences the damping as well. These viscosities are coupled, and cannot be decoupled experimentally by independent adjustment of either the perturbation wave vector k_0 or the amplitude ξ_0. The shear and bulk contributions have different phases, however, so precise measurements of $\phi(t)$ could, at least in principle be analyzed for both shear and bulk viscosities. Such an analysis would be quite sensitive to the initial conditions, however, and the approximations considered here may prove inadequate for this purpose.

Preliminary calculations with the full second-order Navier-Stokes equations for viscous compressible flow indicate that shock instabilities may occur even when the Kontorovich-D'yakov thermodynamic stability criteria are satisfied. These rheological instabilities may manifest themselves as turbulence behind the shock front and might be responsible for the rapid dynamic mixing that is observed in shock-mediated chemical reactions.

Much work evidently remains to be done before shock-wave techniques may be used to obtain reliable measurements of the viscosity of the Earth's outer core, or of silicate liquids in the lower mantle. The prospect is promising, however, and considerable progress has been made in the last $\approx$30 years. We hope that the relevance of this problem to theoretical issues, such as the stability of shock waves, and commercially important processes, such as shock welding and shock chemistry, will stimulate additional interest in this field.

ACKNOWLEDGMENTS

We are grateful to D. W. Schwendeman for his invaluable assistance with the mathematical analysis in Sec. V, and to R. F. Svendsen, Jr. for very helpful discussions regarding the formulation of boundary conditions. We also thank Professor D. J. Stevenson and Professor W. I. Newman for their thoughtful comments and suggestions. This study was supported under NSF Grant No. EAR-8916753, Contribution No. 4884, Division of Geological and Planetary Sciences, California Institute of Technology, Pasadena, CA.

REFERENCES

Alder, B. J., D. M. Gass, and T. E. Wainwright, 1970, J. Chem. Phys. **53**, 3813.
Al'tshuler, L. V., A. A. Bakanova, and R. F. Trunin, 1958, Sov. Phys. Dokl. **3**, 761.
Al'tshuler, L. V., G. S. Doronin, and G. Kh. Kim, 1986, J. Appl. Mech. Tech. Phys. USSR **27**, 887.
Al'tshuler, L. V., G. I. Kanel', and B. S. Chekin, 1977, Zh. Eksp. Teor. Fiz. **72**, 663 [Sov. Phys. JETP **45**, 348 (1977)].
Angell, C. A., P. A. Cheeseman, and S. Tamaddon, 1982, Science **218**, 885.
Bakanova, A. A., V. N. Zubarev, Yu. N. Sutulov, and R. F. Trunin, 1976, Sov. Phys. JETP **41**, 544.
Backus, G., 1968, Philos. Trans. R. Soc. London, Ser. A **263**, 239.
Barker, L. M., 1968, in *Behavior of Dense Media Under High Dynamic Pressures,* IUTAM Symposium (Gordon and Breach, New York), p. 483.
Bellman, R. E., R. E. Kalaba, and J. A. Lockett, 1966, *Numerical Inversion of the Laplace Transform: Applications to Biology, Economics, Engineering, and Physics* (Elsevier, New York).
Bett, K. E., and J. B. Cappi, 1965, Nature **207**, 620.
Bhatia, A. B., 1967, *Ultrasonic Absorption* (Dover, New York).
Bland, D. R., 1965, J. Inst. Math. Appl. **1**, 56.
Boslough, M. B., 1989, Chem. Phys. Lett. **160**, 618.
Boslough, M. B., 1990, J. Chem. Phys. **92**, 1839.
Bottinga, Y., and D. F. Weill, 1972, Am. J. Sci. **272**, 438.
Brey, L. A., G. B. Schuster, and H. G. Drickamer, 1977, J. Chem. Phys. **67**, 2648.
D'yakov, S. P., 1954, Zh. Eksp. Teor. Fiz. **27**, 288.
Förster, Th., and G. Hoffmann, 1971, Z. Phys. Chem. Frankfurt NF, **75**, 63.
Fowles, G. R., and A. F. P. Houwing, 1984, Phys. Fluids **27**, 1982.
Freeman, N. C., 1955, Proc. R. Soc. London, Ser. A **288**, 341.
Fujii, T., and I. Kushiro, 1977a, Carnegie Inst. Washington Yearb. **76**, 419.
Fujii, T., and I. Kushiro, 1977b, Carnegie Inst. Washington Yearb. **76**, 461.
Gans, R. F. , 1972, J. Geophys. Res. **77**, 360.
Godunov, S. K., A. A. Deribas, and V. I. Mali, 1976, Combust. Explos. Shock Waves USSR **11**, 1.
Godunov, S. K., A. A. Deribas, I. D. Zakharenko, and V. I. Mali, 1971, J. Appl. Mech. Tech. Phys. USSR **12**, 114.
Godunov, S. K., Ya. M. Kazhdan, and V. A. Simonov, 1969, J. Appl. Mech. Tech. Phys. USSR **10**, 891.
Grady, D. E., 1977, in *High-Pressure Research,* edited by M. H. Manghnani and S.-I. Akimoto (Academic, New York), p. 389.
Grieve, R. A. F., and R. J. Floran, 1978, J. Geophys. Res. **83**, 2761.

Hamann, S., and M. Linton, 1969, J. Appl. Phys. **40**, 913.
Hansen, J. P., and I. R. McDonald, 1986, *Theory of Simple Liquids* (Academic, New York).
Harris, P., and H. N. Presles, 1981, J. Chem. Phys. **74**, 6864.
Herzfeld, K. F., and T. A. Litovitz, 1959, *Absorption and Dispersion of Ultrasonic Waves* (Academic, New York).
Hoover, W. G., D. J. Evans, R. B. Hickman, A. J. C. Ladd, W. T. Ashurst, and B. Moran, 1980, Phys. Rev. A **22**, 1690.
Hoover, W. G., A. J. C. Ladd, R. B. Hickman, and B. L. Holian, 1980, Phys. Rev. A **21**, 1756.
Huston, A. L., B. L. Justus, and A. J. Campillo, 1985, Chem. Phys. Lett. **122**, 617.
Istrakov, A. G., and V. B. Librovich, 1966, J. Appl. Math. Mech. USSR **30**, 541.
Jacobs, J. A., 1987, *The Earth's Core* (Academic, New York).
Kanzaki, M., K. Kurita, T. Fujii, T. Kato, O. Shimomura, and S. Akimoto, 1987, in *High-Pressure Research in Mineral Physics,* edited by M. Manghnani and Y. Syono (American Geophysical Union, Washington, D.C.), p. 195.
Kim, G. Kh., 1984, J. Appl. Mech. Tech. Phys. USSR **26**, 692.
Knittle, E., and R. Jeanloz, 1989, Geophys. Res. Lett. **16**, 421.
Kontorovich, V. M., 1957, Zh. Eksp. Teor. Fiz. **33**, 1525 [Sov. Phys. JETP **6**, 1179 (1958)].
Kormer, S. B., 1968, Usp. Fiz. Nauk. **11**, 641 [Sov. Phys. Usp. **11**, 229 (1968)].
Kushiro, I., 1976, J. Geophys. Res. **81**, 6347.
Kushiro, I., H. S. Yoder, and B. O. Mysen, 1976, J. Geophys. Res. **81**, 6351.
Kushiro, I., 1977, in *High-Pressure Research Applications in Geophysics,* edited by M. H. Manghnani and S. I. Akimoto (Academic, New York), p. 25.
Kushiro, I., 1978a, Earth Planet. Sci. Lett. **41**, 87.
Kushiro, I., 1978b, Carnegie Inst. Washington Yearb. **77**, 672.
Kushiro, I., 1978c, Carnegie Inst. Washington Yearb. **77**, 675.
Kushiro, I., 1980, in *Physics of Magmatic Processes,* edited by R. B. Hargraves (Princeton University, Princeton, New Jersey), p. 93.
Kushiro, I., 1986, J. Geophys. Res. **91**, 9343.
Landau, L. D., and E. M. Lifshitz, 1959, *Fluid Mechanics* (Pergamon, New York).
Liebermann, L. N., 1949, Phys. Rev. **75**, 1415.
Liu, L., and W. A. Bassett, 1986, *Elements, Oxides, Silicates: High-Pressure Phases with Implications for Earth's Interior* (Oxford University, New York).
Lyzenga, G. A., T. J. Ahrens, W. J. Nellis, and A. C. Mitchell, 1982, J. Chem. Phys. **76**, 6282.
Melosh, H. J., 1990, in *Origin of the Earth,* edited by H. E. Newsom and J. H. Jones (Oxford University, New York), p. 69.
Merrill, R. T., and M. W. McElhinny, 1983, *The Earth's Magnetic Field* (Academic, New York).
Miller, G. H., E. M. Stolper, and T. J. Ahrens, 1991, J. Geophys. Res., in press.
Mineev, V. N., and E. V. Savinov, 1967, Zk. Eksp. Teor. Fiz. **52**, 629 [Sov. Phys. JETP **25**, 411 (1967)].
Mineev, V. N., and E. V. Savinov, 1976, Zk. Eksp. Teor. Fiz. **68**, 1321 [Sov. Phys. JETP **41**, 656 (1976)].
Mineev, V. N., and R. M. Zaidel', 1968, Zh. Eksp. Teor. Fiz. **54**, 1633 [Sov. Phys. JETP **27**, 874 (1968)].
Mitchell, A. C., and W. J. Nellis, 1982, J. Chem. Phys. **76**, 6273.
Pistorius, C. W. F. T., M. C. Pistorius, J. P. Blakey, and L. J. Admiraal, 1963, J. Chem. Phys. **38**, 600.
Rayleigh, Lord, 1910, Proc. R. Soc. London, Ser. A **84**, 247.
Razorenov, S. V., G. I. Kanel', O. R. Osipova, and V. E. Fortov, 1987, High Temp. USSR **25**, 57.
Rice, M. H., and J. M. Walsh, 1957, J. Chem. Phys. **26**, 824.
Rigden, S. M., T. J. Ahrens, and E. M. Stolper, 1988, J. Geophys. Res. **93**, 367.
Rochester, M. G., 1970, in *Earthquake Displacement Fields and the Rotation of the Earth,* edited by L. Mansinha, D. Smylie, and A. Beck (Reidel, Dordrecht, Holland), p. 136.
Ryan, M. P., and J. Y. K. Blevins, 1987, U.S. Geol. Surv. Bull. **1764**, 1.
Sakharov, A. D., R. M. Zaidel', V. N. Mineev, and A. G. Oleinik, 1965, Sov. Phys. Doklady **9**, 1091.
Scarfe, C. M., B. O. Mysen, and D. Virgo, 1979, Carnegie Inst. Washington Yearb. **78** , 547.
Schlichting, H., 1979, *Boundary-Layer Theory,* Seventh Ed. (McGraw-Hill, New York).
Schroeder, R. C., and W. H. McMaster, 1973, J. Appl. Phys. **44**, 2591.
Suzuki, Y., and R. Sato, 1970, J. Phys. Earth **18**, 157.
Swan, G. W., G. E. Duvall, and C. K. Thornhill, 1973, J. Mech. Phys. Solids **21**, 215.
Swegle, J. W., and D. E. Grady, 1985, J. Appl. Phys. **58**, 692.
Truesdell, C., and R. A. Toupin, 1960, in *Handbuch der Physik,* edited by S. Flügge (Springer, Berlin), Vol. III/1, p. 226.
Walden, P., 1906, Z. Phys. Chem. **55**, 207.
Woodcock, L. V., C. A. Angell, and P. Cheeseman, 1976, J. Chem. Phys. **65**, 1565.
Yakusheva, O. B., V. V. Yakushev, and A. N. Dremin, 1972, in *Combustion and Explosion* (Izdat. Nauk).
Zaidel', R. M., 1958, J. Appl. Math. Mech. USSR **24**, 316.
Zaidel', R. M., 1967, J. Appl. Mech. Tech. Phys. USSR **8**, 30.
Zel'dovich Ya. B., and Yu. P. Raizer, 1967, *Physics of Shock Waves and High-Temperature Hydrodynamic Phenomena* (Academic, New York).